



High Performance Lithium Ion-Conducting Plasticized Biopolymer Electrolyte for Supercapacitor Application

M. Nandhinilakshmi¹ · D. Vanitha^{1,2} · N. Nallamuthu³ · K. Sundaramahalingam⁴ · P. Saranya¹ · Shameem Abdul Samad⁵

Accepted: 8 May 2024

© The Author(s), under exclusive licence to Springer Science+Business Media, LLC, part of Springer Nature 2024

Abstract

Lithium-ion based Solid Polymer Electrolytes are synthesized by incorporating lithium perchlorate (LiClO_4) salt with Iota-Carrageenan (IC) / Acacia Gum (AG) plasticized with ethylene glycol (EG) by solution casting method. The X-ray diffraction and Fourier transform infrared analysis are used to analyze the structural and molecular complexation. From the AC impedance analysis spectra, it is found that the incorporation of 15 wt% of LiClO_4 salt into a blend polymer electrolyte (IAO15) shows the maximum ionic conductivity of 2.02×10^{-2} S/cm and minimum activation energy (0.022 eV). The conduction mechanism for IAO15 sample follows two models (CBH and QMT). The dielectric and modulus spectra confirm the non-Debye nature of the sample. From the Transference Number Measurement, it is observed that the conductivity is due to Li ions and IAO15 sample is chosen for the fabrication of a Symmetrical supercapacitor. At 3.6 Ag^{-1} current density, the power and energy densities are noted as 7452 Wkg^{-1} and 165.6 Whkg^{-1} respectively.

Keywords XRD · AC impedance · GCD · LSV · Lithium perchlorate · Supercapacitor

Introduction

Over the past few decades, researchers have focused on energy conversion and energy storage devices from renewable energy sources. Fossil fuels are going to be exhausted eventually, because of the worldwide energy consumption [1, 2]. Compared with the other energy storage devices, supercapacitors are used in a variety of industries, including

telecommunications, medical equipment, and electric vehicles because of their low cost, high power density, and prolonged cycle life [3]. The active components of supercapacitors such as electrodes, electrolyte, and separator have significant effects on their electrochemical performance. Generally metal oxides and carbon-based materials are used as electrode materials [4]. Then the polymer-based electrolytes are preferred for solid state electrochemical application.

Compared with synthetic polymers, biopolymers are gained popularity due to its environmental concerns. But it has low conductivity and numerous techniques are used to improve their conductivity [5]. Researchers have explored various biopolymers such as chitosan [3], starch [6], pectin [7], carrageenan [8], agar-agar [9], methylcellulose [10], and cellulose acetate [11]. In particular, these biopolymers are economical and it is a good substitute for synthetic polymers in a variety of electrochemical applications. Carrageenan stands out among them as a suitable host polymer because of its water solubility property and contains specific functional groups within its structure [12]. Carrageenan can be categorized into three types: Iota, Lambda, and Kappa based on the positioning and number of ester sulfate groups. The composition of Iota-carrageenan has monomers of

✉ D. Vanitha
vanibala2003@gmail.com

¹ Multi-Functional Materials Laboratory, International research center, Kalasalingam Academy of Research and Education, Srivilliputhur, Tamilnadu 626 126, India

² Department of Physics, Kalasalingam Academy of Research and Education, Srivilliputhur, Tamilnadu 626 126, India

³ Department of Physics, Dayananda Sagar Academy of Technology and Management, Bangalore, Karnataka 560082, India

⁴ Department of Physics, Arulmigu Kalasalingam College of Arts and Science, Krishnan Kovil, Tamilnadu 626 126, India

⁵ Department of Science and Humanities, Centre for Energy and Environment, Karpagam Academy of Higher Education, Coimbatore 641021, India

β -D-galactopyranose and α -D-galactopyranose, connected by α -(1 \rightarrow 3) and β -(1 \rightarrow 4) glycosidic linkages [13]. The conductivity of pure IC electrolyte is observed as 3.86×10^{-6} S cm $^{-1}$.

A popular method used by researchers to improve the conductivity is polymer blending [14, 15]. As a part of identifying a polymer for blend, gum based polymer stands in a suitable place. The various types of gums are Acacia gum (also referred to as AG), Guar gum [16], Tragacanth gum [17], Gellan gum [18], Moringa gum [19] and Xanthan gum [20]. Among them, AG is a Polysaccharide which is derived from the gum exudate of the Acacia tree. It possesses a complex, highly branched polysaccharide structure with glycoprotein constituents. Gum Arabic is widely available and finds predominant use as an emulsifying agent, stabilizer, and thickener [21]. AG is composed of 4-O-methyl glucuronic acid units that are joined with β -glycosidic linkage. It includes D-galactose, D-glucuronic acid, L-arabinose, and L-rhamnose at an appropriate molar ratio [22]. It is simple to blend Arabic gum with another polymer.

Plasticizers are incorporated into membranes to increase flexibility, smooth texture, and improve the chemical and mechanical strength of the membranes. These additives have the ability to penetrate or increase the spacing between molecules, thereby reduce the polar groups found in polymers [23, 24].

Since lithium is the lightest metal, it is frequently chosen as a doping salt due to its huge potential window, small cationic and large anionic sizes, high redox potential, and high gravimetric Coulombic density. Ongoing efforts are directed towards the advancement of novel ion-conducting polymer electrolytes suitable for lithium-based energy devices. Incorporating a lithium salt with an ion-conducting biopolymer matrix has been proposed as a potential replacement for liquid electrolytes in lithium-ion batteries and supercapacitors [25, 26]. It has less electronegativity compared with other fluoro type salts [27, 28].

In this work, Lithium Perchlorate (LiClO $_4$) is selected as a dopant owing to its low dissociation energy, low lattice energy (723 kJ/mol). As per the earlier reports of LiClO $_4$ based biopolymer electrolytes, higher ionic conductivity of 1.7×10^{-4} S cm $^{-1}$ is reported by Sudiarti, T. et al., for cellulose acetate with 10% LiClO $_4$ [29]. Y. M. Yusof and M. F. Z. Kadir has also reported that the plasticized blend biopolymer electrolyte of methylcellulose /potato starch doped with LiClO $_4$ has attained the maximum ionic conductivity of 4.2×10^{-4} S cm $^{-1}$ [30]. As per the earlier reports, LiClO $_4$ is selected as a suitable dopant salt with the selected blend.

In this work, LiClO $_4$ doped plasticized biopolymer blend electrolytes has prepared and achieved the conductivity in the order of 10^{-2} S cm $^{-1}$. By using the higher conductivity

biopolymer electrolyte, symmetric capacitors are fabricated and their properties are discussed.

Experimental

Materials

Iota carrageenan (IC) and acacia gum (AG) were obtained from Qualigens Fine Chemicals Pvt., Ltd. and Himedia Chemicals (HiMedia Laboratories Pvt., Ltd.), respectively. The AG monomer has a molecular weight of 92 g/mol with SQ grade, whereas the IC monomer has a molecular weight of 946.8 g/mol with 99% purity. Pure ethylene glycol with a molecular weight of 62.07 g/mol was purchased from Merck Specialities Private Limited with 99% purity. TCS Pvt. Ltd. supplied lithium perchlorate (LiClO $_4$) with a molecular weight of 106.39 g/mol with AR grade purity. Deionized water was taken as the solvent throughout the procedure. The necessary materials for preparing the electrodes such as N-methyl pyrrolidone (NMP), poly(vinylidene fluoride) (PVdF), and activated carbon were purchased from SANWA Components, Inc.

Experimental Details

Plasticized blend biopolymer electrolytes (PBE) were synthesized by a technique called solution casting method. The solution casting technique is also known as the direct casting method most commonly used to prepare polymeric films which are utilized across various fields of material science and engineering. The method involves the dissolution of the polymers in suitable solvents. The polymeric solutions, which may contain various additives, such as plasticizers and crosslinkers (e.g., genipin and glutaraldehyde), are evaporated [31]. Hence, many authors regard this method as the conventional solution casting method. For the preparation of electrolytes, it is preferred to select this method as it serves as a simple method [6, 32].

After dissolving the IC in 40 ml of deionized water, the mixture was heated to 60 °C for three hours. By using 20 ml of deionized water, AG polymer was dissolved at an ambient temperature. Using a magnetic stirrer, both solutions were gently mixed and stirred for 3 h to form a clear solution. Then 0.75 ml of ethylene glycol (plasticizer) was added to this blend solution. Concurrently, 10 ml of distilled water were used to dissolve different concentrations of LiClO $_4$ (5wt.%, 10wt.%, 15wt.%, and 20wt.%), which were then agitated for two hours at room temperature. After adding the salt solution to the plasticized polymer blend solution, the mixture was left to agitate for 20 h. After that, a Petridis was filled with the clear solution, which was then placed in an

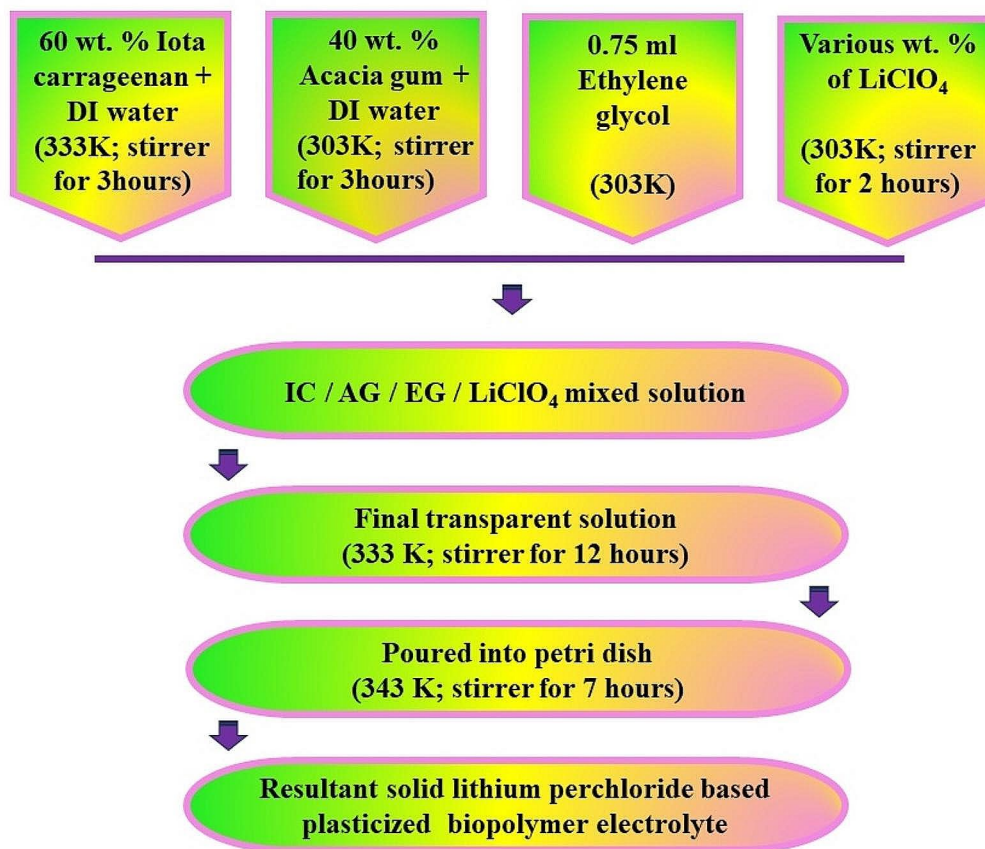


Fig. 1 Schematic diagram of electrolyte preparation

Table 1 Prepared samples ratio in grams and weight%

S.no	Sample code	The ratio of IC: AG: LiClO ₄ weight% with 0.75 ml Ethylene glycol	Ratio in grams
1	IAB	60:40:00	0.936:0.063:0.000
2	IAO05	57:38:05	0.932:0.060:0.008
3	IAO10	54:36:10	0.921:0.062:0.017
4	IAO15	51:34:15	0.913:0.062:0.026
5	IAO20	50:30:20	0.905:0.061:0.034

oven set at 60° C to evaporate. A schematic representation of the electrolyte synthesis of a polymer electrolyte sample is shown in Fig. 1. As shown in Table 1, the sample codes are IAO05, IAO10, IAO15, and IAO20. The salt content rises as a 5wt.%, 10wt.%, 15wt.%, and 20wt.% ratio.

Symmetrical Electrode Preparation

To prepare the electrodes, N-methyl pyrrolidone (NMP), poly(vinylidene fluoride) (PVdF), and activated carbon are taken in the proportion of 8:1:1. PVdF, NMP and activated carbon were mixed together using a pestle and mortar to produce a homogenous mixture. Once the mixture was ready, it was spread out onto nickel foil and dried for 12 h at

80 °C. In order to avoid moisture, the electrodes were kept in a desiccator.

Analytical Methods and Characterization Techniques

The amorphous nature of the plasticized biopolymer electrolytes is confirmed by the X-ray diffraction pattern acquired from a Bruker X-ray diffractometer. Cu-K α radiation is used for the diffraction scan, which covers the 2 θ range of 10°–60° at a rate of 5°/min. A computer-controlled HIOKI 3532-50 LCR Hi tester is used in the determination of ionic conductivity and dielectric characteristics. The tests are conducted at frequencies between 42 and 1 MHz in the temperature range of 303–368 K. Using a CH-Instrument Model 6008e, electrochemical performance is examined using cyclic voltammetry (CV) and galvanostatic charge/discharge (GCD) techniques. Moreover, the Wagner polarization technique is used to calculate the transference number.

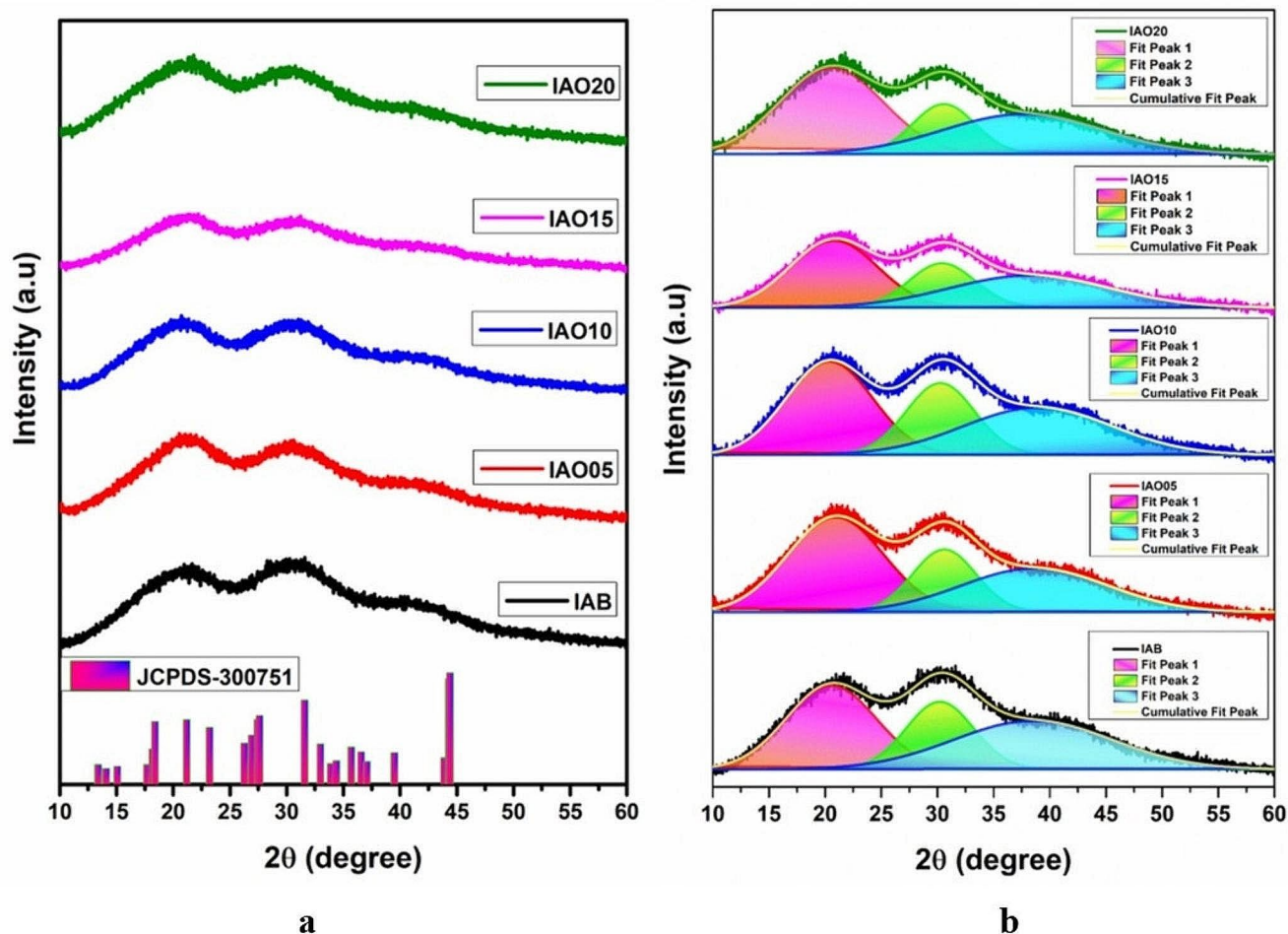


Fig. 2 a XRD pattern for the Plasticized blend polymer electrolyte and LiClO_4 , b X-ray deconvolution for all prepared samples

Results and Discussion

X-Ray Diffractometer

The diffraction pattern of optimized electrolyte (IAB) and different wt% of LiClO_4 incorporated electrolytes are shown in Fig. 2a. The existence of IC and AG in the optimized blend sample IAB is confirmed from the X-ray diffractogram. The humps located at $2\theta = 20^\circ$, 30° , and 40° are presented in IAB [13]. While increasing the salt concentration, the intensity of these humps at $2\theta = 20^\circ$ and 32° gets decreased up to IAO15 which confirms the improvement in the amorphous nature of the electrolyte. For IAO20 sample, the intensity of the humps is increased. There is no distinct crystalline peaks associated with lithium perchlorate (according to the JCPDS-30-0751 database) in all the samples which represents the complete dissolution of the ionic dopant in the polymer blend system [33]. The good amorphous nature or disorder occurred in the lithium

Table 2 The calculated degree of crystallinity from XRD spectra

Sample code	Degree of Crystallinity (%)
IAB	38
IAO05	36
IAO10	35
IAO15	32
IAO20	34

incorporated polymer membranes improves the polymer segmental motion [29, 34].

As shown in Fig. 2b, the Origin deconvolution technique is used for the determination of the crystallinity. The following formula is used to find the degree of crystallinity (χ_c).

$$\chi_c(\%) = \frac{A_c}{A_T} \times 100 \quad (1)$$

where, A_c is the area of crystalline peaks and A_T is the total area (the addition of crystalline and amorphous peaks area) of the XRD data [35]. Table 2 displays the calculated degree of crystallinity. The variation in the values by increasing

LiClO_4 salt concentration denotes the change in amorphous nature of the polymer electrolytes. The lowest crystallinity of 32% is noted for the sample IAO15.

FTIR

The FTIR method examines the interaction among the chemical compounds of the blended polymer with the LiClO_4 and the EG. Changes in the vibrational modes of molecules are attributed to the interactions between atoms or ions within the polymer electrolyte system as detailed in Table 3. The FTIR pattern in the wavenumber range of 4000 to 400 cm^{-1} is shown in Fig. 3. By the addition of LiClO_4 salt, the vibrational peak at 3354 cm^{-1} is shifted to 3348 cm^{-1} , indicating the existence of a hydroxyl group in IAB (blend electrolyte) [8]. The observed vibration peak at 2932 cm^{-1} in all solid polymer electrolytes (SPEs) is associated with the C–H stretching vibration [36]. A distinct vibrational peak at 1635 cm^{-1} signifies the H–O–H deformation band in salt-doped samples. The intensity of this peak diminishes with the addition of salt [13]. At 1438 cm^{-1} , a vibrational peak is appeared which corresponds to the symmetrical and asymmetrical stretching of $-\text{COO}-$. But for the IAO15 sample, it is shifted to 1460 cm^{-1} [37]. The distinctive shifts in these

Table 3 FTIR peak assignments for all the prepared SPEs

Assignments	Wave-number (cm^{-1})
O–H Stretching	3348
C–H Stretching	2934
H–O–H (Water deformation band)	1645
$-\text{COO}-$ symmetrical and asymmetrical Stretching	1460
S–O sulfate stretching	1232
C–O stretching of 3–6 anhydro galactose stretching	1067
CH_2 asymmetric stretching	1032
C–O–C of 3–6 anhydro galactose stretching	926
$-\text{O}-\text{SO}_3$ stretching at D-galactose-4-sulphate	848
Sulfate C–4 galactose	736
ClO_4^- Stretching	693

peaks indicate the complexation between Li^+ ions and oxygen atoms in the polymer backbone [29].

The peak observed at 1224 cm^{-1} is due to S–O sulfate stretching in all the prepared samples. The vibrational peaks at 1064 cm^{-1} and 1032 cm^{-1} are attributed to the C–O stretching of 3–6 anhydro galactose and CH_2 asymmetric stretching [38]. The transmittance peak at 920 cm^{-1} is associated with C–O–C stretching in 3–6 anhydro-galactose [34]. Additionally, the vibrational peaks at 842 cm^{-1} and

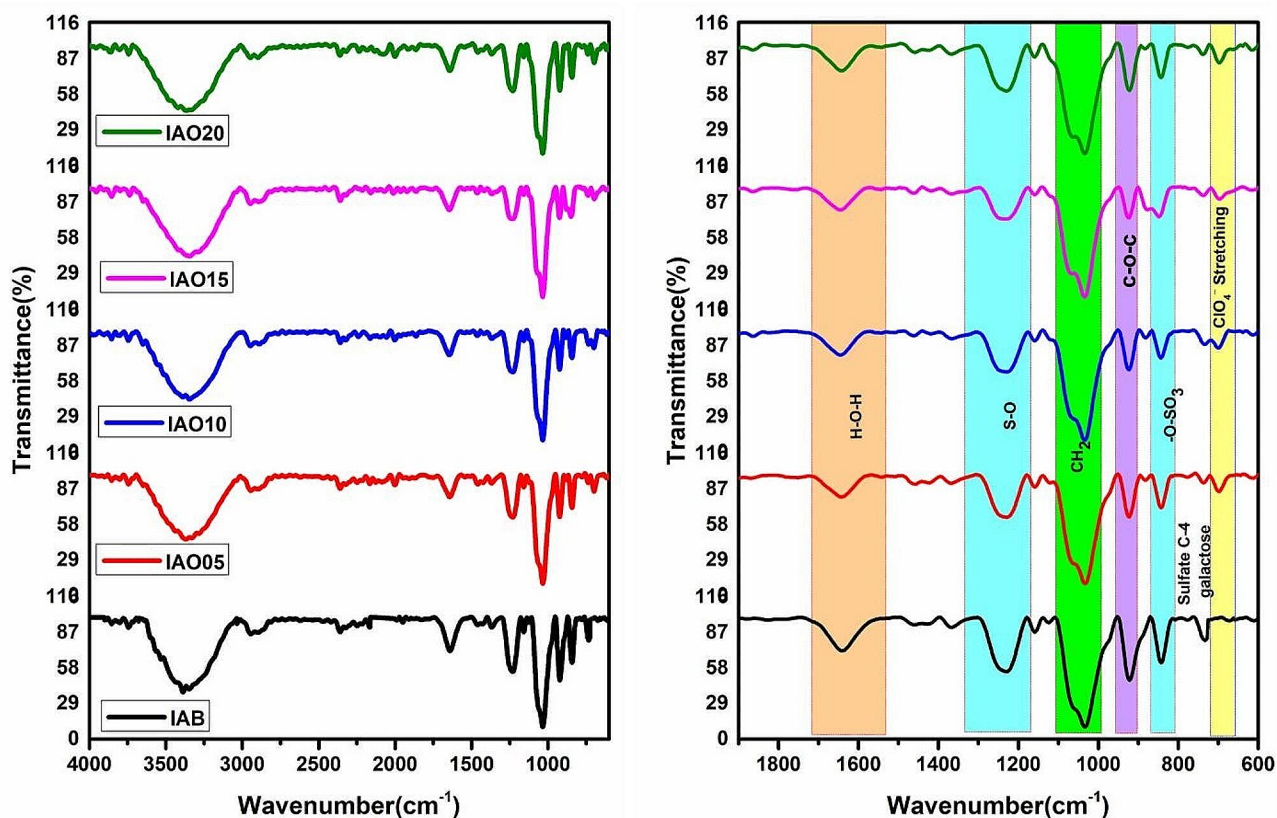


Fig. 3 FTIR spectra of the Plasticized blend polymer electrolyte and LiClO_4 salt added electrolyte system

738 cm^{-1} correspond to $-\text{O}-\text{SO}_3$ stretching in D-galactose-4-sulphate and sulfate C-4 galactose. The impact of the interaction between LiClO_4 and blend polymer electrolyte at 738 cm^{-1} is also related to C-Cl vibrations [7]. The solvated-separated ion pair (Li^+ -solvent- ClO_4^-) that occurs in the prepared electrolyte is indicated by the shift in the peak at 697 cm^{-1} that results from the free ClO_4^- anion. The intensity of this transmittance peak is decreased with salt concentration. For the sample IAO20, the intensity of the peak is increased [7, 39, 40].

Cole–Cole

AC impedance spectroscopy is used to analyze the ionic conductivity as well as dielectric properties of biopolymer electrolytes. Zview software is used to determine the bulk resistance (R_b) of the electrolytes [27]. The prepared polymer electrolytes are analyzed using Cole–Cole plots with equivalent circuits, as shown in Fig. 4a–e. Generally, Cole–Cole plots reveal two distinct zones owing to the bulky nature of the electrolytes. A semicircular pattern occurs in the high-frequency region due to the combined action of bulk resistance along with bulk capacitance and a spike observed at low-frequency is due to the blocking electrode. These features are attributed to the polarizing process occurring at the electrolyte-electrode interface [41, 42].

The Cole–Cole plot for the IAB electrolyte is characterized by a semicircle with a spike. The corresponding circuit

includes a series resistance and a parallel combination of resistance and capacitance phase element (QPE), followed by another series connection of QPE. The impedance analysis of the IAO05, IAO15 and IAO20 sample confirms the existence of two semicircles with a spike. The equivalent circuit model contains a parallel combinations of resistance (R) and capacitance with QPE₁, QPE₂ and QPE₃ as depicted in Fig. 4c, e and f. For the sample, IAO10 shows two semicircles and the circuit is given in Fig. 4d. The presence of two semicircles is due to the enhanced molecular packing of the iota carrageenan polymer chain [8].

The sample IAO15 has the lowest bulk resistance value and high ionic conductivity. Although the addition of salt more than 15 wt%, LiClO_4 results in poor mobility which increase the bulk resistance and decrease the ionic conductivity. The calculation of ionic conductivity (σ) for the salt-incorporated biopolymer electrolytes is performed by the given equation,

$$\sigma = \left(\frac{1}{R_b}\right) \times \left(\frac{t}{A}\right) \text{Scm}^{-1} \quad (2)$$

Where ‘t’ denotes the thickness of the electrolyte, Area of the electrolyte is ‘A’ is, and ‘ R_b ’ represents the bulk resistance of the electrolyte [43]. Figure 4a reveals that the bulk resistance (R_b) experiences a notable reduction up to 15wt. % of LiClO_4 incorporated sample (IAO15). Remarkably, the IAO15 sample demonstrates a high conductivity value of

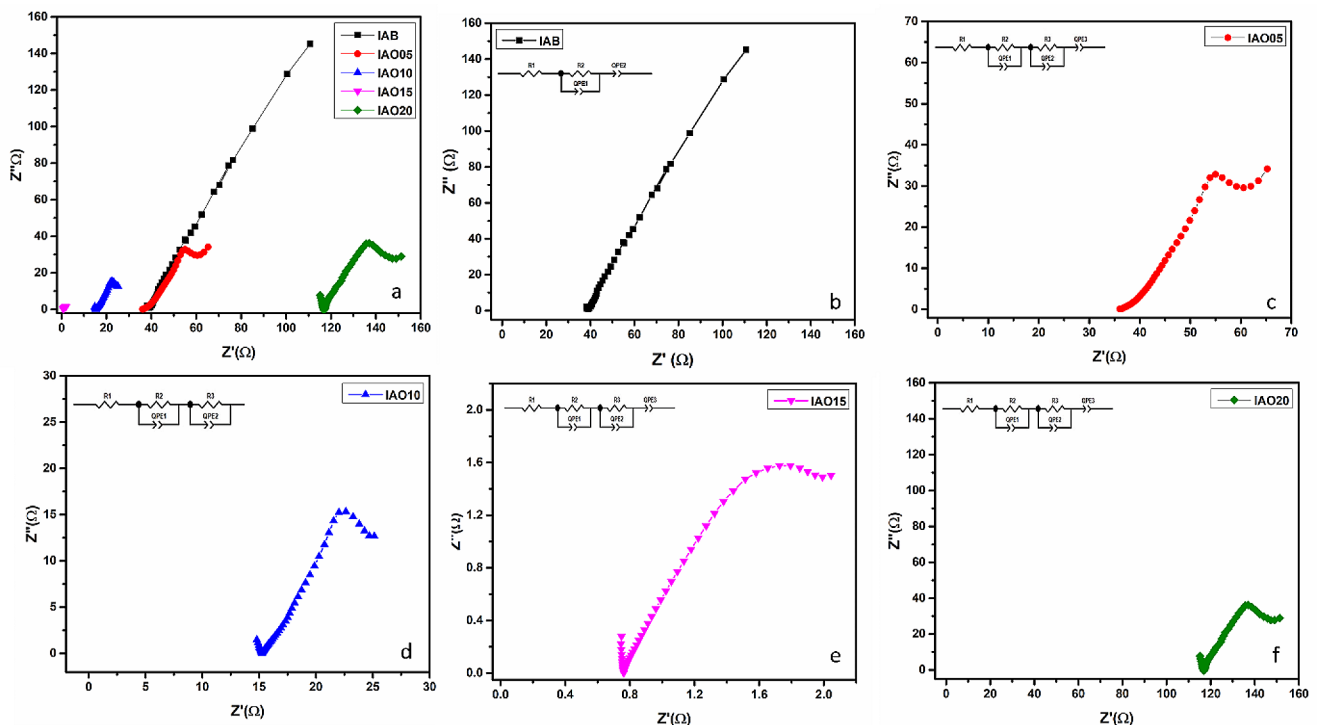


Fig. 4 a–f Cole–Cole plot of the Plasticized blend polymer electrolyte and LiClO_4 salt added electrolyte system

Table 4 Measured conductivity and activation energy values of all samples

Sample code	AC Conductivity (Scm ⁻¹)	DC Conductivity (Scm ⁻¹)	Activation energy (eV)
IAB	2.96×10^{-4}	3.98×10^{-4}	0.071
IAO05	5.02×10^{-4}	5.13×10^{-4}	0.066
IAO10	1.33×10^{-3}	1.08×10^{-3}	0.062
IAO15	2.02×10^{-2}	1.99×10^{-2}	0.022
IAO20	1.22×10^{-4}	1.16×10^{-4}	0.075

$2.02 \times 10^{-2} \text{ S cm}^{-1}$. When the salt concentration is increased to 20 wt% (IAO20), the resistance increases and thereby the conductivity decreases. Ionic conductivity values for these polymer electrolytes obtained by the Cole–Cole plot are presented in Table 4.

Conduction Mechanism

Several theoretical models can be used to relate the temperature dependency of frequency exponent (s). For the higher conducting electrolyte sample IAO15, the plot of s versus temperature is shown in Fig. 5. The simultaneous forward and backward motion of ions causes an increase in conductivity at higher frequencies which increases ion mobility. The conduction follows the power law which is explained by the following Eq. [44].

$$\sigma_{ac} = \sigma_{dc} + A\omega^s \quad (3)$$

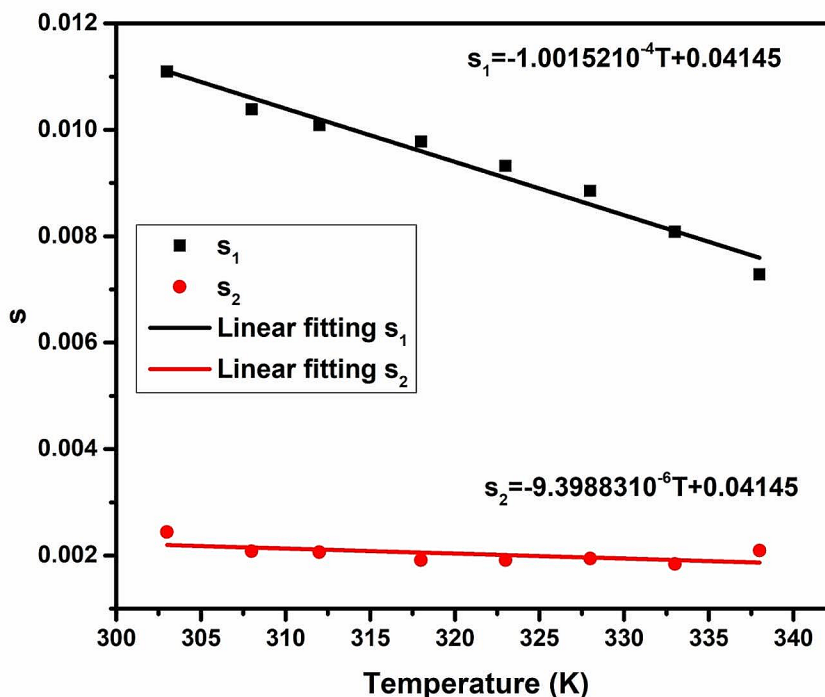
$$\omega^s = \frac{S_{dc}}{A} \quad (4)$$

Here, hopping frequency is represented by ' ω^s ', and temperature-dependent parameter is represented by ' A '. Typically, the power law exponent (s) tends to be less than one [45]. The various types of conduction mechanism includes Overlapping large polaron tunnelling (OLPT), Non-overlapping small polaron tunnelling (NSPT), Quantum mechanical tunnelling (QMT), and Correlated barrier hopping (CBH) [8].

From Fig. 5, there are two exponents s_1 and s_2 which corresponds to Region I and Region II. With an increase in temperature, s_1 tends to decrease. This implies that solid polymer electrolyte system follows the CBH model. In the CBH model, it is believed that charge carriers are encompassed by various potentials, including the repulsive force between ions (known as the coulombic repulsive potential) as well as a potential well. As explained by Buraidah et al., while the ions acquire sufficient energy, they transit or “hop” from one location to another. The ions can either return to their initial state (back-hop) or establish a new potential with a higher barrier for hopping back which enable them to continue moving forward [15].

In the second region, s_2 follows the QMT model. In this model, there is no change (constant) in s value which means s value is independent of temperature. According to the QMT model, the conducting proton and stress fields combine to

Fig. 5 Conduction mechanism of the higher conducting sample IAO15



produce the polaron. The polarons move by the tunneling process through the potential barrier. AC conductivity is increased by atomic or electron tunneling between equilibrium sites [46, 47]. The plot of exponents s_1 and s_2 against T can be fitted by the equations, $s_1 = -1.00152 \times 10^{-4} T + 0.04145$ and $s_2 = -9.39883 \times 10^{-6} T + 0.04145$.

Arrhenius Behavior

Figure 6 illustrates the Arrhenius characteristics of all the prepared electrolytes. As the temperature increases, the conductivity of the prepared polymer electrolyte also increases. The relationship between the activation energy (E_a) and conductivity (σ) is explained by Arrhenius behavior using the equation,

$$\sigma = \sigma_0 e^{\{-E_a/(K_b T)\}} \quad (5)$$

T is the temperature, and K_b denotes Boltzmann's constant. The plot shows that as the temperature rises, the conductivity also increases. This is due to the increase in the number density and mobility of ions with the increase in temperature [15]. The ion hopping mechanism guides the migration of ions within this electrolyte system. Since the proportion of salt rises, the activation energy decreases for the samples 5wt. % LiClO_4 , 10wt. % LiClO_4 and 15wt. % LiClO_4 . The higher conducting polymer electrolyte IAO15 has a minimum activation energy of 0.022 eV compared with the other electrolytes which suggests the requirement of lower energy for migration for higher conducting samples [15]. For the sample IAO20, the activation energy is increased to 0.075 eV as given in Table 4.

Dielectric Studies

A fundamental way to investigate the ion storage mechanism in polymer composites is to estimate the values of dielectric

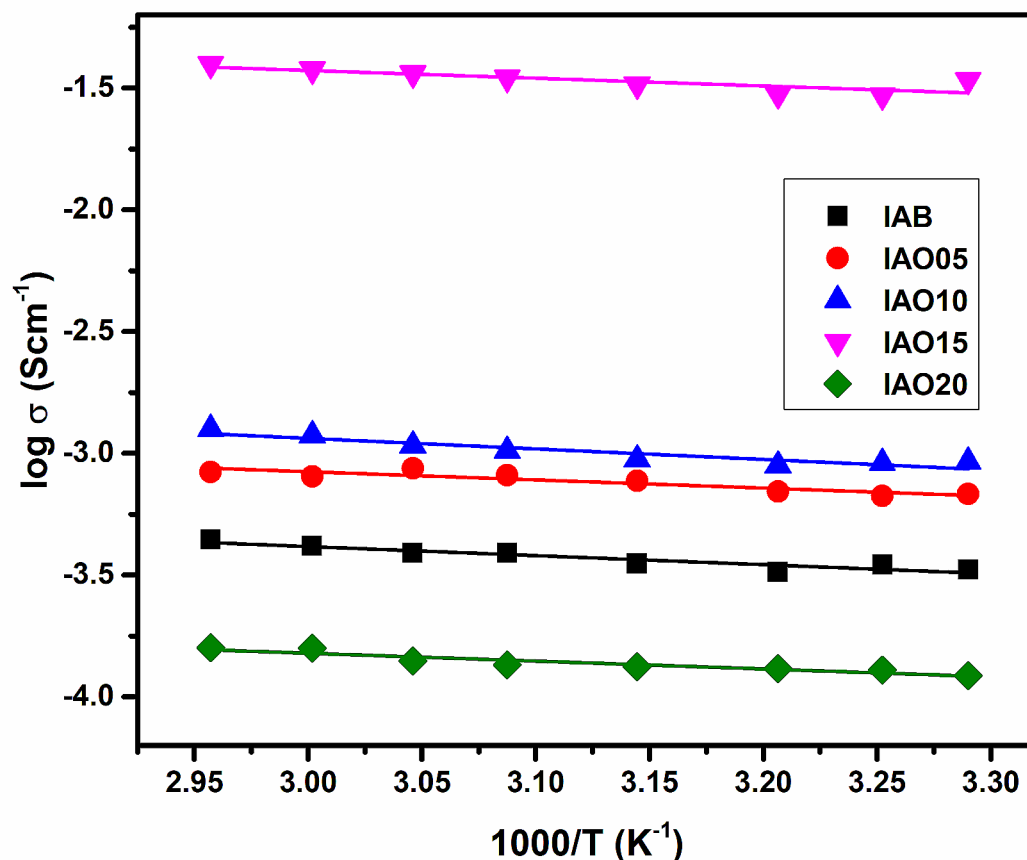


Fig. 6 Temperature-dependent conductivity plot for the blend electrolyte and LiClO_4 salt-added electrolyte system

constant and loss. Dielectric characteristics of SPEs are demonstrated by the plot between real (ϵ') and imaginary parts (ϵ'') of complex permittivity. The following equations are used for the determination of dielectric permittivity,

$$\epsilon^* = \epsilon' - j\epsilon'' \quad (6)$$

$$\epsilon' = \left(\frac{Z''}{\omega C_0 (Z'^2 + Z''^2)} \right) \quad (7)$$

$$\epsilon'' = \left(\frac{Z'}{\omega C_0 (Z'^2 + Z''^2)} \right) \quad (8)$$

Where, ϵ^* means complex permittivity, ϵ' is the real dielectric permittivity, ϵ'' denotes imaginary dielectric permittivity, ω is the angular frequency, C_0 represents vacuum capacitance while real and imaginary parts of impedance are represented by Z' and Z'' [48]. Figures 7 and 8 shows the

dielectric constant and loss of all the prepared samples. ϵ' is used for the determination of dipole orientation or polarization and ϵ'' represents the energy required for the alignment of dipoles [14].

It is noticeable that the dielectric constant and loss are maximum at the low frequency. At high frequency, ϵ' and ϵ'' are minimum and reached a constant value. In contrast to other SPEs, the higher conducting sample IAO15 exhibits a maximum value of ϵ' and ϵ'' at low frequencies due to space charge polarization and the free Li-ions accumulation at the electrode-electrolyte interface [49, 50]. The values ϵ' and ϵ'' are constant at high frequencies, indicating that there is no chance for charge carriers to align themselves with the field direction. Furthermore, there is less diffusion of charge carriers in the direction of the field [51, 52].

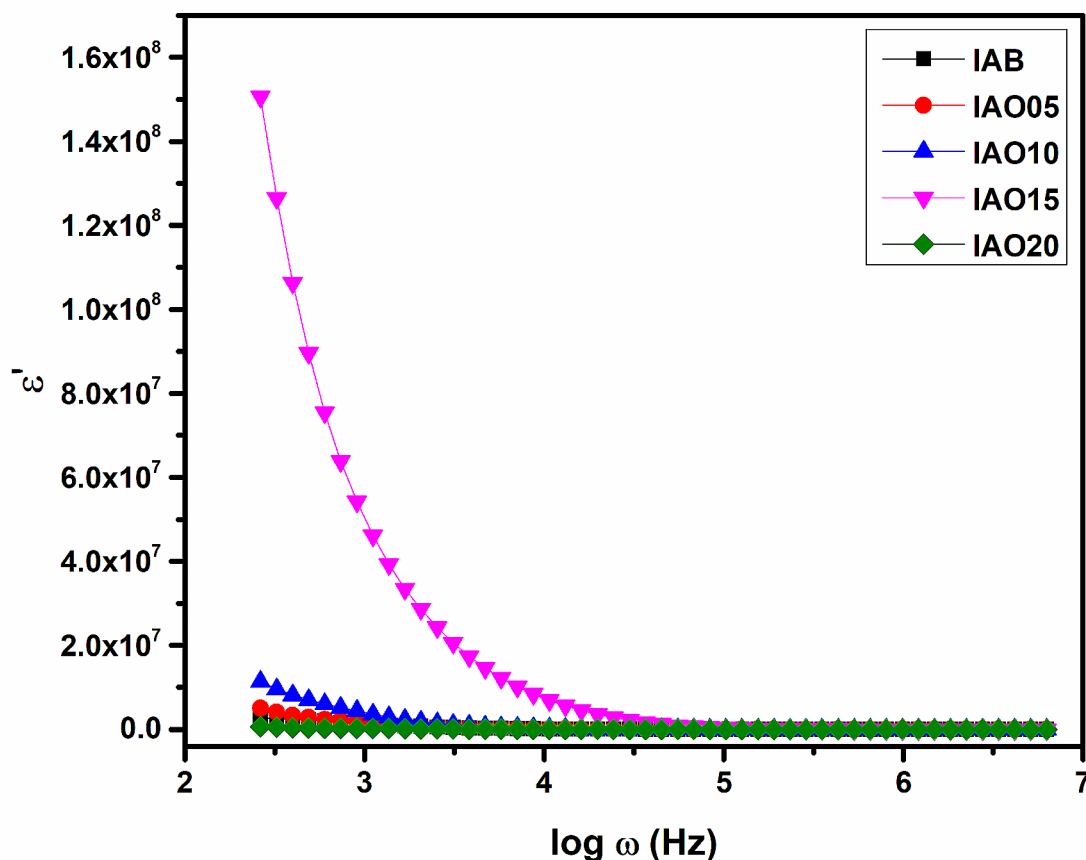


Fig. 7 Dielectric constant versus log frequency for the blend electrolyte and LiClO_4 salt added electrolyte system

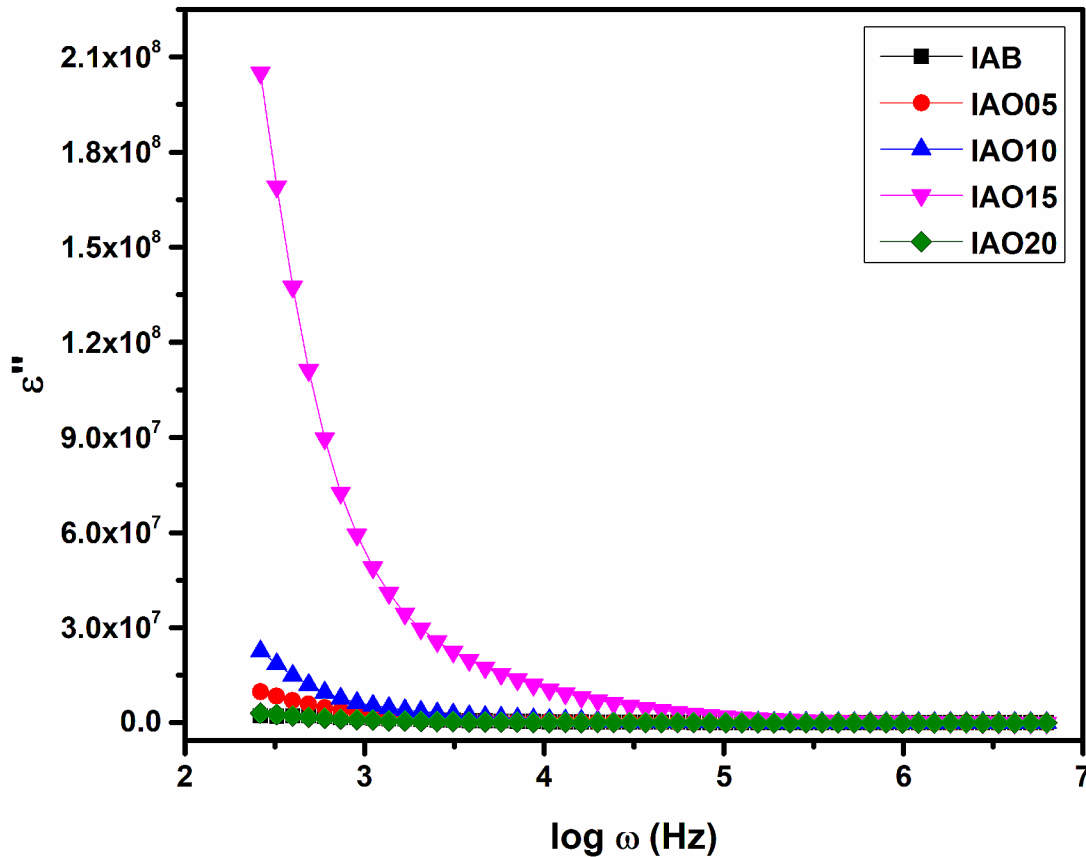


Fig. 8 Dielectric loss versus log frequency for the blend electrolyte and LiClO_4 salt added electrolyte system

Modulus Spectra

The reciprocal of complex relative permittivity is explained as the electric modulus, it is particularly helpful for analyzing electrical relaxation processes. The frequency-dependent real and imaginary parts of dielectric modulus spectra M' and M'' for all the prepared samples are shown in Figs. 9 and 10. The equations are given as,

$$M^* = \frac{1}{\epsilon^*} \quad (9)$$

$$M' = \left(\frac{\epsilon'}{\epsilon'^2 + \epsilon''^2} \right) \quad (10)$$

$$M'' = \left(\frac{\epsilon''}{\epsilon'^2 + \epsilon''^2} \right) \quad (11)$$

Here, ϵ' and ϵ'' denotes real and imaginary parts of dielectric permittivity [53]. At the low frequencies, M' and M'' approaches zero. This confirms the high capacitive behavior and the lack of the restoring force that typically governs the movement of charge carriers in the presence of an electric field [54]. There is an improvement in the real M' and imaginary M'' part of modulus values as improving the frequency, suggesting the impact of the bulk effect. These findings provide an evidence to support the existence of non-Debye characteristics in the samples [55].

Tangent Spectra (Dissipation Factor δ)

The frequency-dependent dielectric loss tangent spectra is shown in Fig. 11. The dielectric relaxation time of all the LiClO_4 added samples is calculated and given in Table 5. The shift in the loss tangent peak towards higher frequencies occurs with an increase in salt content. A process of dielectric relaxation is indicated by this change. The value of $\tan\delta$

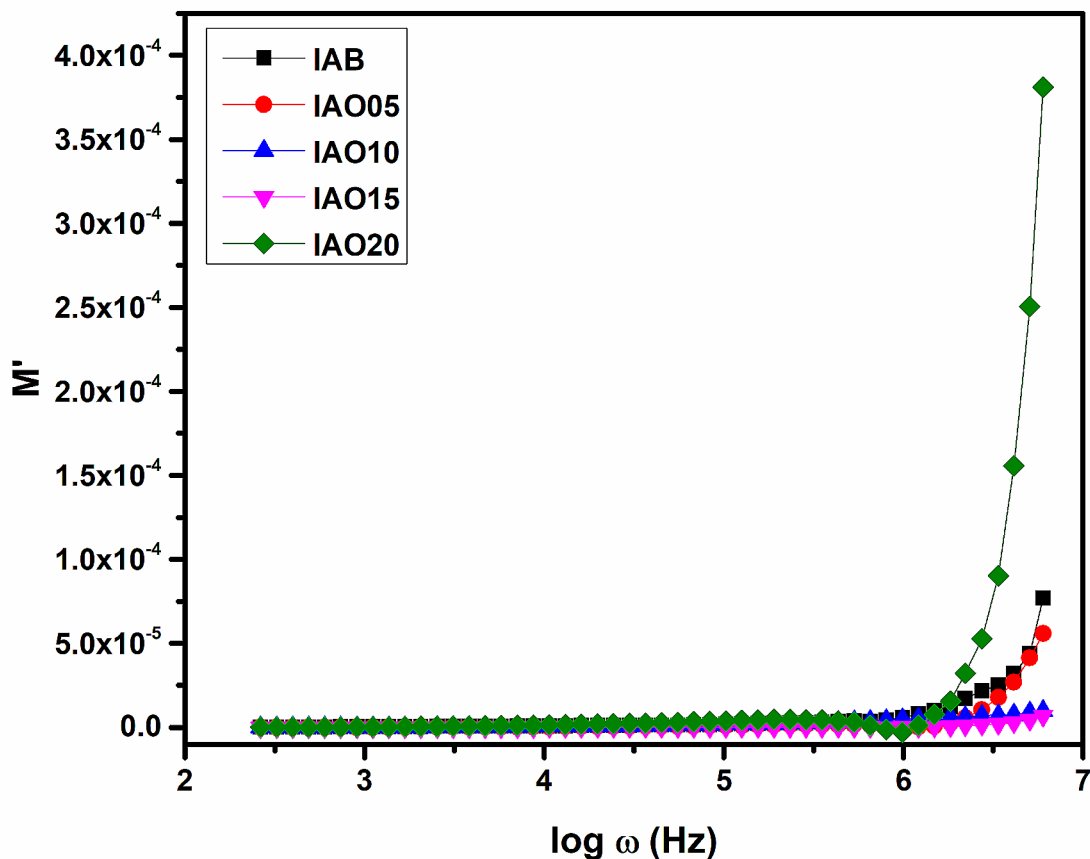


Fig. 9 Real dielectric modulus spectra versus log frequency for the blend electrolyte and LiClO_4 salt added electrolyte system

reaches a maximum value and drops with the increase in frequency. The translational ion dynamics associated with the dielectric relaxation in mobile ions is represented by the peak. The rise of $\tan \delta$ with frequency may be explained by a fluctuation in the quantity of reactive (capacitive) and active (ohmic) components [32, 56]. The loss tangent is determined by,

$$\tan \delta = \frac{\epsilon'}{\epsilon''} \quad (12)$$

$$\tau = \frac{1}{2\pi f} = \frac{1}{\omega} \quad (13)$$

In this above equation, ϵ' and ϵ'' denotes real (constant) and imaginary (loss) parts of dielectric permittivity respectively. τ denotes the relaxation time and ω is the angular frequency obtained from loss tangent spectra by peak and baseline

fitting. The existence of relaxation time is the consequence of the effort carried out by the ionic charge carriers within the polymer electrolyte to follow the change in the direction of the applied field. With an increase in salt concentration, the height of the peak increases, and the $\tan \delta$ peaks shift to a higher frequency. This suggests quicker relaxation time. The addition of the lithium perchlorate salt upto 15 wt%, the ionic conductivity increases by the enhancement of the number of carrier ions and the movement of ions. This leads to improvement of transport properties in the IAO15 electrolyte, as the combination of instant segmental motion and mobile ions facilitates to faster ion transport. For this reason, when conductivity increases, the relaxation time value become reduces [57].

The value of relaxation time (τ) is calculated and the minimum τ value is observed as 5.54×10^{-7} s for the higher conducting τ sample IAO15. In Table 5, τ values are tabulated for all the prepared electrolyte.

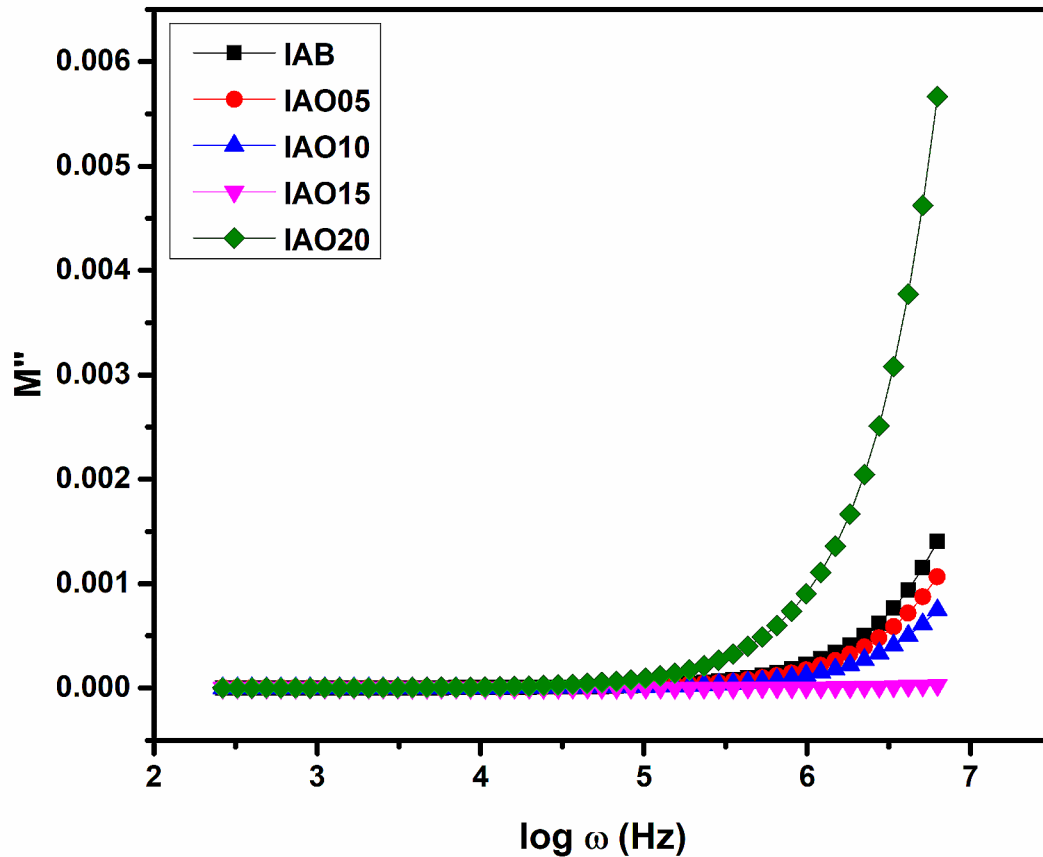


Fig. 10 Imaginary dielectric modulus spectra versus log frequency for the blend electrolyte and LiClO_4 salt added electrolyte system

Transference Number Analysis

Wagner's DC polarization approach is used to calculate the transference numbers by using blocking electrodes. The current flow is noted until it reaches a steady-state saturation. Figure 12 illustrates the polarization current of the LiClO_4 dopant system over time. Using a working voltage of 2 V, the initial high value of the current is attributed to the coexistence of two charges: electrons and ions. This initial current undergoes a sudden decrease over time. The " t_{ion} " and " t_{ele} " values are calculated using the formula,

$$t_{\text{ion}} = [(I_i - I_f) / I_i] \quad (14)$$

$$t_{\text{ele}} = (1 - t_{\text{ion}}) \quad (15)$$

Where t_{ion} is the transference number of ions, t_{ele} represents the transference number of electrons, I_f represents the final

current, I_i represents the initial current. Table 6 shows the obtained transference number values. The t_{ion} value for all salt-added electrolyte systems are within the range of 0.97–0.99. In this analysis, the t_{ion} is found to be high (0.99) for the IAO15 sample. The polymer-ion and ion-ion interactions may be the reason for the high transference number [58, 59]. From the transference numbers (t_{ele} and t_{ion}) and conductivity (σ) values, the subsequent parameters are determined by the following Eq.

$$D = D_+ + D_- = \frac{KTs}{ne^2} \quad (16)$$

$$t_{\text{ion}} = \frac{D_+}{D_+ + D_-} \quad (17)$$

$$t_{\text{ele}} = \frac{D_-}{D_+ + D_-} \quad (18)$$

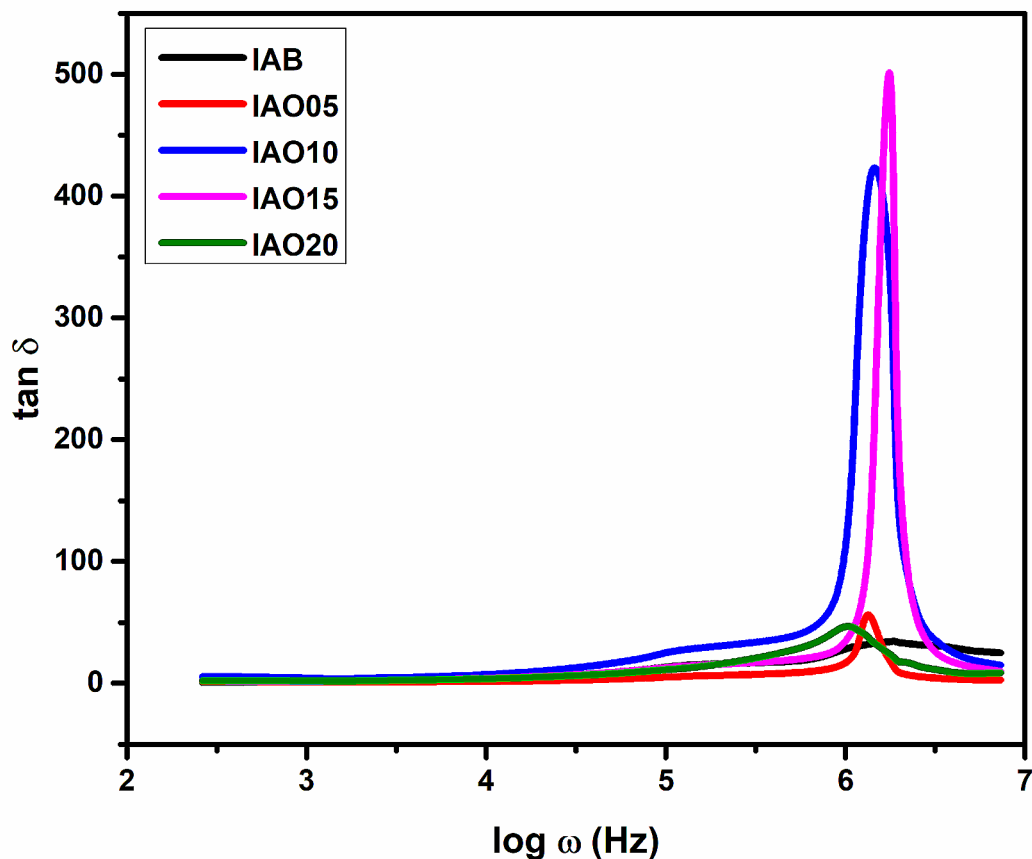


Fig. 11 Loss tangent spectra versus log frequency for the blend electrolyte and LiClO_4 salt added electrolyte system

Table 5 Observed tangent spectra parameters

Sample code	Relaxation time (τ) in s
IAB	6.72×10^{-7}
IAO05	7.74×10^{-7}
IAO10	7.05×10^{-7}
IAO15	5.54×10^{-7}
IAO20	1.04×10^{-6}

$$\mu = \mu_+ + \mu_- = \frac{\sigma}{ne} \quad (19)$$

$$t_{ion} = \frac{\mu_+}{\mu_+ + \mu_-} \quad (20)$$

$$t_{ele} = \frac{\mu_-}{\mu_+ + \mu_-} \quad (21)$$

In these equations, D denotes diffusion coefficient (cm^2/s), μ means mobility (cm^2/Vs), ρ =Density of the salt ($\text{LiClO}_4=2.42 \text{ g/cm}^3$), Boltzmann constant is denoted as K

($K = 1.38 \times 10^{-23} \text{ m}^2 \text{ kg s}^{-2} \text{ K}^{-1}$), σ represents Conductivity (S cm^{-1}), e is the Charge of the electron ($1.602 \times 10^{-19} \text{ C}$), n is the number of charge carriers and N represents Avogadro's number (6.023×10^{23} particles per mole) [8].

A comparison of D_+ and μ_+ values for cations and D^- and μ^- values for anions reveals that the former are larger. Anions' and cations' mobility as well as the diffusion coefficient exhibit the comparable behaviour with the SPEs' conductivity, which rises upto IAO15. Furthermore, the transference number of the cation is never approached to unity, revealing that there is some anionic presence in the total ionic conductivity [60].

Fabrication

The fabrication of a symmetrical capacitor involves the assembly of two identical electrodes (activated carbon) and an electrolyte (IAO15). Using galvanostatic

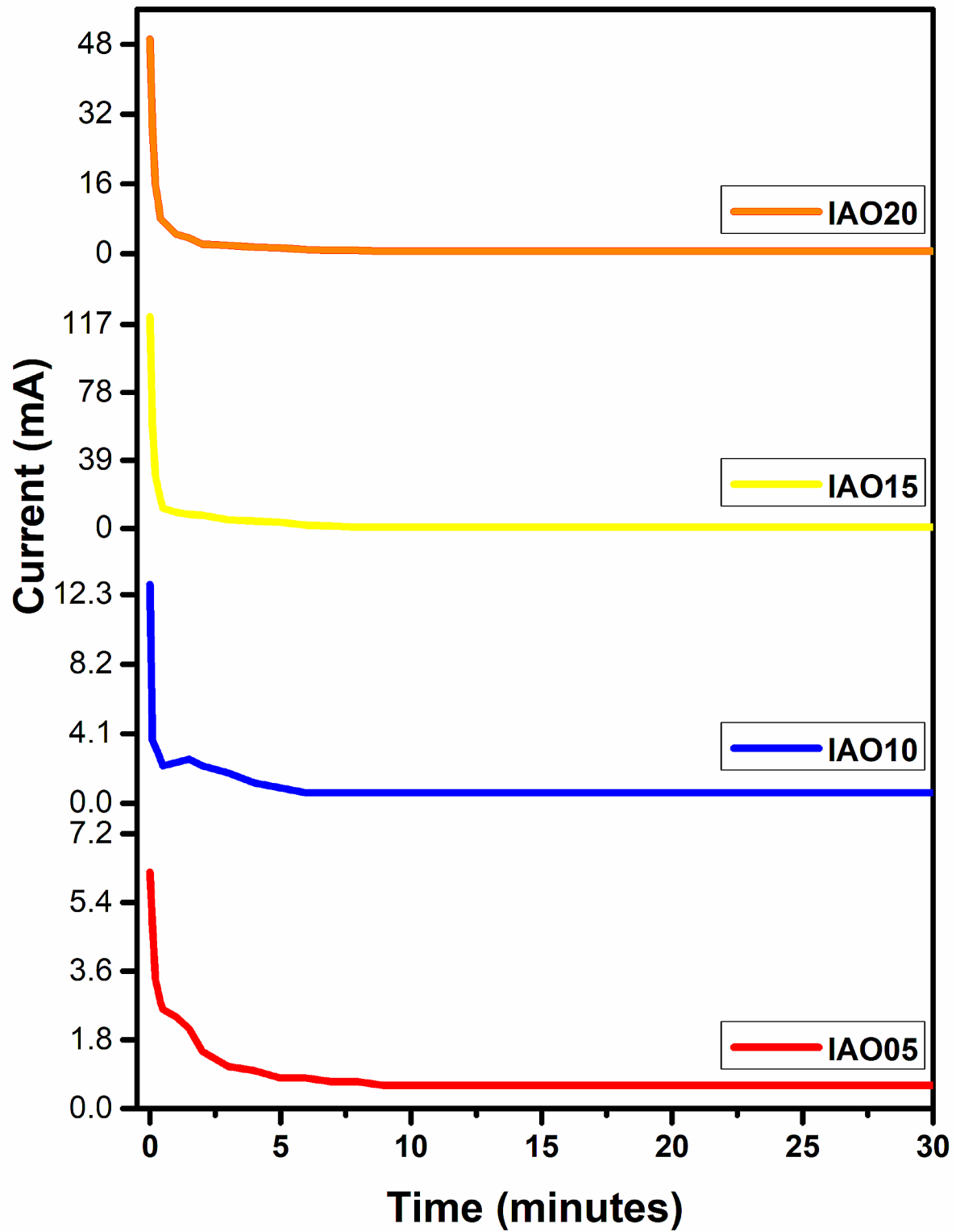


Fig. 12 Wagner DC polarization plot for the samples IAO05, IAO10, IAO15 and IAO20 at ambient temperature

Table 6 Mobility and diffusion coefficient of prepared solid polymer electrolyte

Wt.% of LiClO ₄	No. of charge carriers (n) in cm ⁻³ (10 ¹⁹)	Transference Number		Diffusion co-efficient in cm ² /s			Mobility (μ) in cm ² /Vs		
		T _{ion}	T _{elec}	D (10 ⁻⁶)	D ₊ (10 ⁻⁶)	D ₋ (10 ⁻⁹)	μ (10 ⁻⁵)	μ ₊ (10 ⁻⁵)	μ ₋ (10 ⁻⁷)
5	5.16	0.9758	0.0241	0.159	0.15	3.85	0.61	0.59	1.47
10	10.3	0.9535	0.0465	0.211	0.20	9.79	0.81	0.77	3.75
15	15.5	0.9995	0.0005	2.13	2.13	1.07	8.16	8.15	0.41
20	20.6	0.9613	0.0387	0.009	0.009	0.37	0.04	0.04	0.14

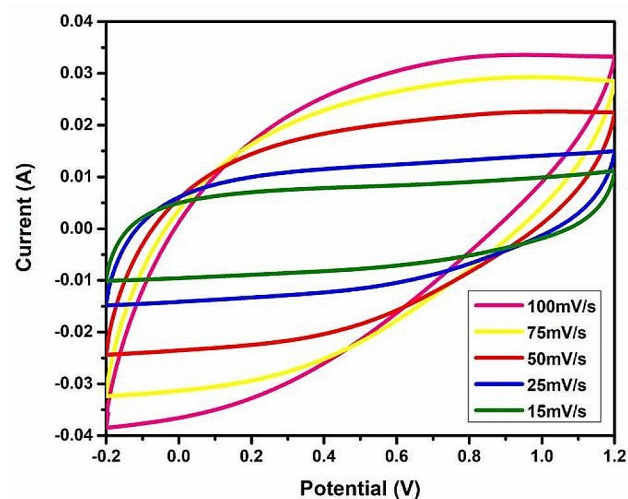
Table 7 The calculated device's, specific capacitance, power density, energy density, and area

Cyclic Voltammetric		Galvanostatic Charge-Discharge (GCD)		
C _s (F/g)	Current density (A/g)	C _s (F/g)	Power density (W/kg)	Energy density (Wh/kg)
367	2.4	292	1380	54
464	2.8	275	5796	182
577	3.2	261	6624	173
761	3.6	250	7452	166
901	16 (1st cycle)	75	8000	12

charge-discharge (GCD) and cyclic voltammetry (CV) tests, the electrochemical characteristics of this supercapacitor are measured.

Cyclic Voltammetry

Using an IAO15 sample, a symmetric capacitor is constructed, and cyclic voltammetry (CV) analysis is used to examine its electrochemical performance. Figure 13a depicts the symmetric capacitor's CV curve in the potential range -0.2 to 1.2 V for different scan rates between 15 and 100 mV/s. An electric double-layer capacitor's (EDLC) behaviour is indicated by the CV plot's leaf-like form.

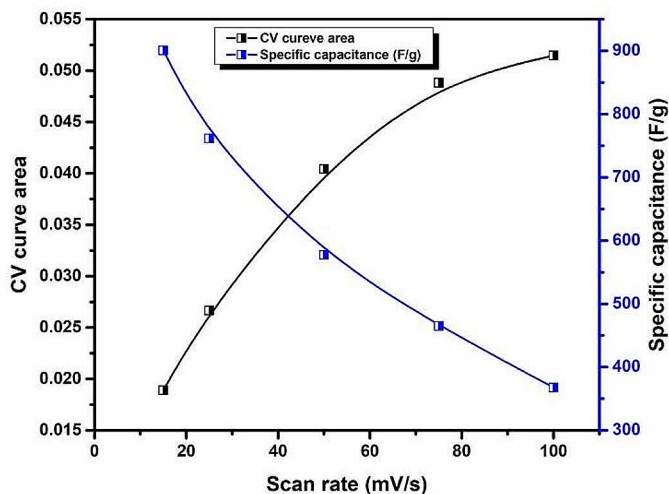


The following equation is used to get the EDLC specific capacitance.

$$C_{spe} = \frac{\int_{V_i}^{V_f} IdV}{vm(V_f - V_i)} \quad (22)$$

The system's initial and final voltages are represented by the variables V_i and V_f respectively. The letters m , v , and $\int IdV$ stands for the mass of the active material, scan rates, and the actual area under the CV curve [61].

The absence of a redox peak in the cyclic voltammetry (CV) profile is attributed to the migration of anions (ClO⁻) and cations (Li⁺) from the LiClO₄ salt at the activated carbon electrodes interface, rather than following an intercalation/deintercalation mode [62]. Table 7 presents specific capacitance values at various scan rates. With increasing scan rates, the curve surface area also increases, signifying effective ion migration. This recommends that sample IAO15 is suitable for EDLC. Figure 13b shows the relationship between specific capacitance and curve area with scan rate. The device's specific capacitance decreases as the scan rate increases, particularly at a low scan rate of 15 mV/s, the specific capacitance value of the EDLC is 901 Fg⁻¹.

**Fig. 13** a CV curves of devices at different scan rates, b Comparison of specific capacitance and area for the devices

GCD

Figure 14a and b, demonstrates the GCD curves and the relationship between current density and specific capacitance for a symmetrical capacitor. The Galvanostatic Charge-Discharge (GCD) curves represent how the applied current relates to voltage throughout a symmetrical capacitor's charge and discharge study. In the initial section of the discharge curve, a slight potential drop is observed, commonly referred to as self-discharge.

When assessing electrochemical supercapacitor performance, the calculations of energy and power density are vital. It is important to note that power density and energy density are not always directly correlated. Even though a device may have a lower power density, it can still operate for a considerable duration if it possesses a higher energy density.

The calculations for energy and power density can be determined using the following relationship:

$$E = \frac{1}{2}CV^2 \quad (23)$$

$$P = \frac{E}{\Delta t} \quad (24)$$

The discharging time is denoted by Δt (in seconds) and the potential window by V (in volts). At a current density of 2.4 A/g, the symmetrical capacitor exhibits an energy density of 54 Wh/kg. As the current density increases, the maximum energy density is noted as 166 Wh/kg. Table 6 displays the calculated values for energy density and power density.

From Fig. 15, the initial energy density (E_d) at the first cycle is determined as 12 Whkg⁻¹. Subsequently, the E_d

Values show a Decline, Reaching a Relatively Constant Value of 6.67 Whkg⁻¹ by the 1000th cycle. There is a slight variation in resistance for anions and cations to traverse from the first cycle to the thousandth. Despite a minor decline in the energy dissipation (E_d value) over these cycles, there is an increase in Equivalent Series Resistance (ESR). This leads to a higher loss of stored energy during charge-discharge cycles [63, 64].

According to the findings of Aziz and colleagues, they developed an EDLC (Electrochemical Double Layer Capacitor) device using a chitosan (CS): poly (ethylene oxide) (PEO): LiClO₄ electrolyte system. This device exhibits a specific capacitance of 6.88 Fg⁻¹. Moreover, when the device is subjected to 100 complete cycles at a current density of 0.5 mAcm⁻², it exhibits a power density of 305 Wkg⁻¹ and an energy density of 0.94 Whkg⁻¹ [65]. Yusof et al. [62], synthesized a solid polymer electrolyte system using a methyl cellulose-potato starch polymer blend with LiClO₄ as a dopant salt and glycerol as a plasticizer. The researchers obtained a C_{sp} value of 28.04 F g⁻¹ and tested the EDLC for 1000 cycles.

The Prepared symmetric capacitor attained a specific capacitance of 292.2 Fg⁻¹ at a current density of 2.4 Ag⁻¹. This capacitor's galvanostatic charge-discharge time (t) is 140 s. At 3.6 Ag⁻¹ current density, it has energy density and power density values of 7452 Whkg⁻¹ and 165.6 Wkg⁻¹, respectively. The findings from this work are comparable with the earlier literature and demonstrates the high electrochemical behavior of the prepared electrolyte.

It is observed that lower current density results in higher energy density, while higher current densities lead to lower energy density. Initially, the achieved power density (P_d) is 8000 Wkg⁻¹. For the subsequent cycles as indicated in Fig. 16, constant P_d is maintained during charge-discharge.

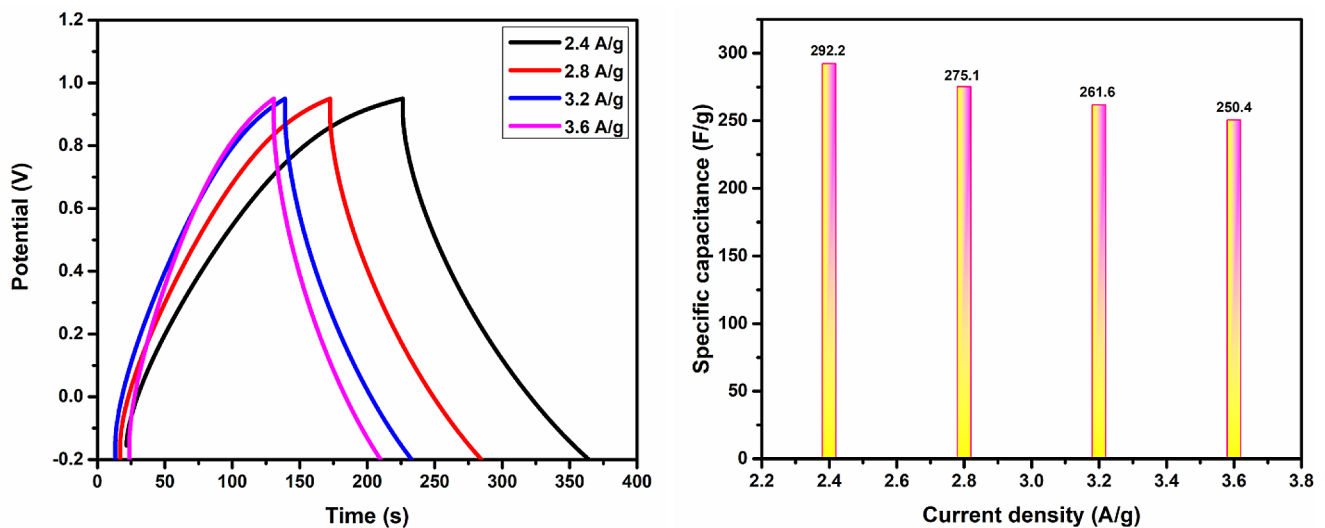


Fig. 14 a GCD curves of devices at different current density and b current density vs. specific capacitance relation of EDLC

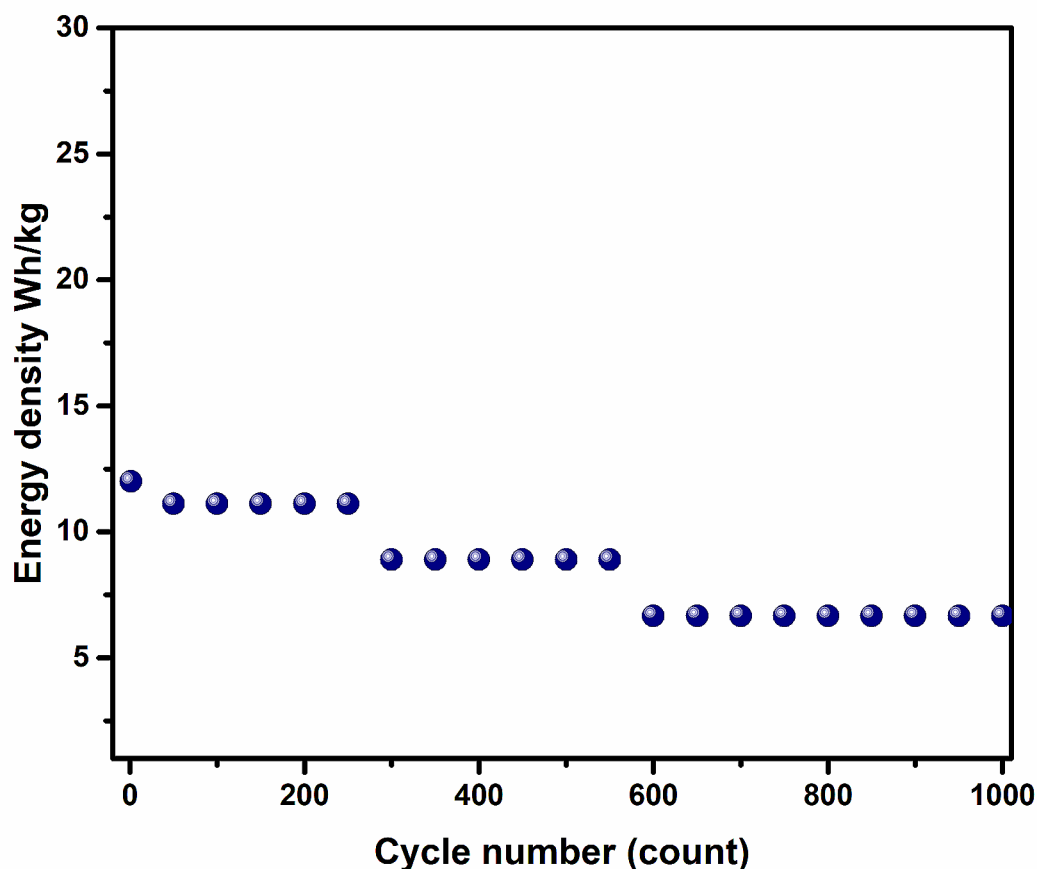


Fig. 15 Energy density (E_d) for the fabricated symmetric capacitor throughout 1000 cycles

Rapid charge-discharge induces an ion aggregation and impedes the ion flow to the electrode surface. Consequently, ion adsorption at the electrode-electrolyte interface decreases [8].

The formula for calculating the internal resistance or equivalent series resistance (ESR) of a symmetric capacitor is,

$$\text{ESR} = V_d/I \quad (25)$$

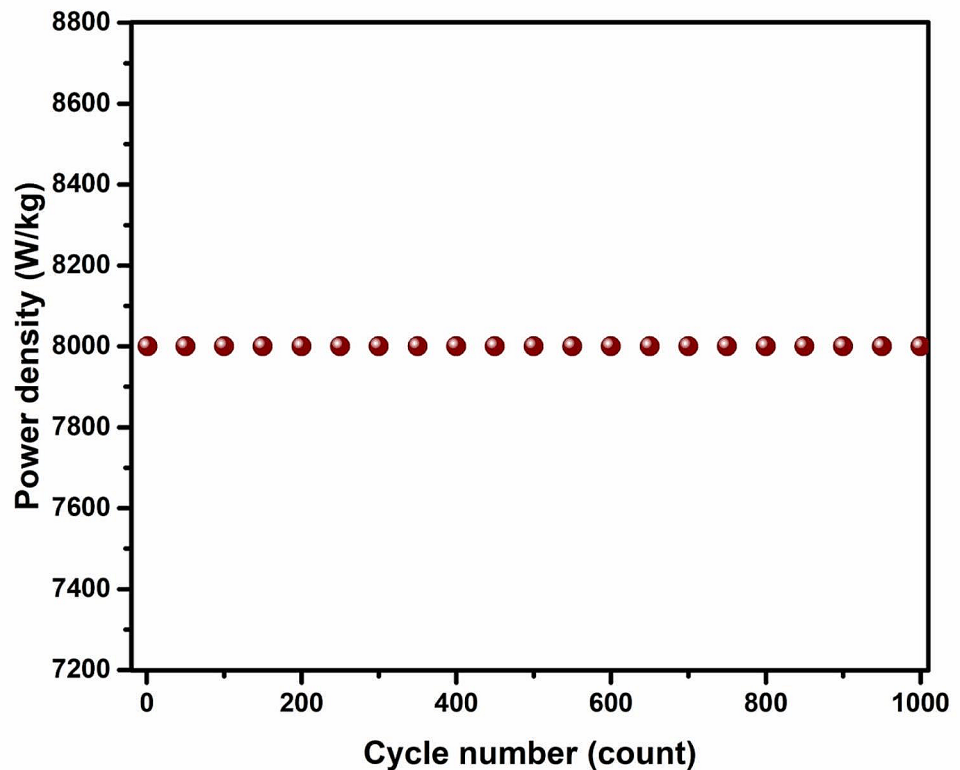
where V_d is the voltage drop. Figure 17 indicates that the R_{ESR} value is changed during a period of 1000 cycles. R_{ESR} value of 284 ohms is recorded at the beginning of the first cycle. As the cycle count increases, the R_{ESR} value shows a slight change. These fluctuations in the R_{ESR} value are associated with the change in the voltage drop. The voltage drop caused by internal resistance within the EDLC is divided into three resistances: the current collector, the

bulk resistance of the electrolyte, and the interfacial region between the electrode and the electrolyte [63, 66].

Conclusions

Using solution casting technique, a transparent plasticized biopolymer electrolyte containing iota carrageenan, Acacia gum, ethylene glycol and LiClO_4 was synthesized. The XRD data shows that the prepared electrolytes are amorphous in nature by the addition of salt. From the FTIR spectra, the complexation of blend polymer electrolyte with Li^+ ions and oxygen molecules is denoted by the presence of the band at 1460 cm^{-1} for the sample IA015. Presence of LiClO_4 in all the samples is confirmed by ClO_4^- stretching vibrations at 697 cm^{-1} region. From the AC impedance study, the higher ionic conductivity is achieved for IA015 sample as $2.02 \times 10^{-2} \text{ Scm}^{-1}$. This sample follows the QMT and CBH models as mentioned in conduction mechanism. The

Fig. 16 Power density (P_d) for the fabricated symmetric capacitor throughout 1000 cycles



higher conducting sample IAO15 sample obeys the Arrhenius behavior and has a low activation energy of 0.022 eV. Dielectric parameters increase by the addition of salt upto 15 wt% (IAO15). From tangent spectra (δ), the minimum relaxation time is observed as 5.54×10^{-7} s for the IAO15 sample. Transport of Li ions ($t_{\text{ion}}=0.99$) are the main reason for the maximum conductivity value, which is confirmed by the Wagner's polarization method. A Symmetrical super capacitor is fabricated by using the higher conducting electrolyte. The Electrochemical properties of the symmetric capacitor is analyzed by the cyclic voltammetry (CV). The curves demonstrate non-faradaic reactions which makes the supercapacitor ideal for energy storage purposes. At 2.4 Ag^{-1} current density, this supercapacitor exhibits a specific capacitance of 292 Fg^{-1} . At a current density of 3.6 Ag^{-1} , power and energy densities are calculated and reported as 7452 Wkg^{-1} and 165.6 Whkg^{-1} respectively. The calculated values are compared with the earlier literature and prove that the prepared electrolyte has good electrochemical property and makes the sample as a promising choice for symmetrical capacitor applications.

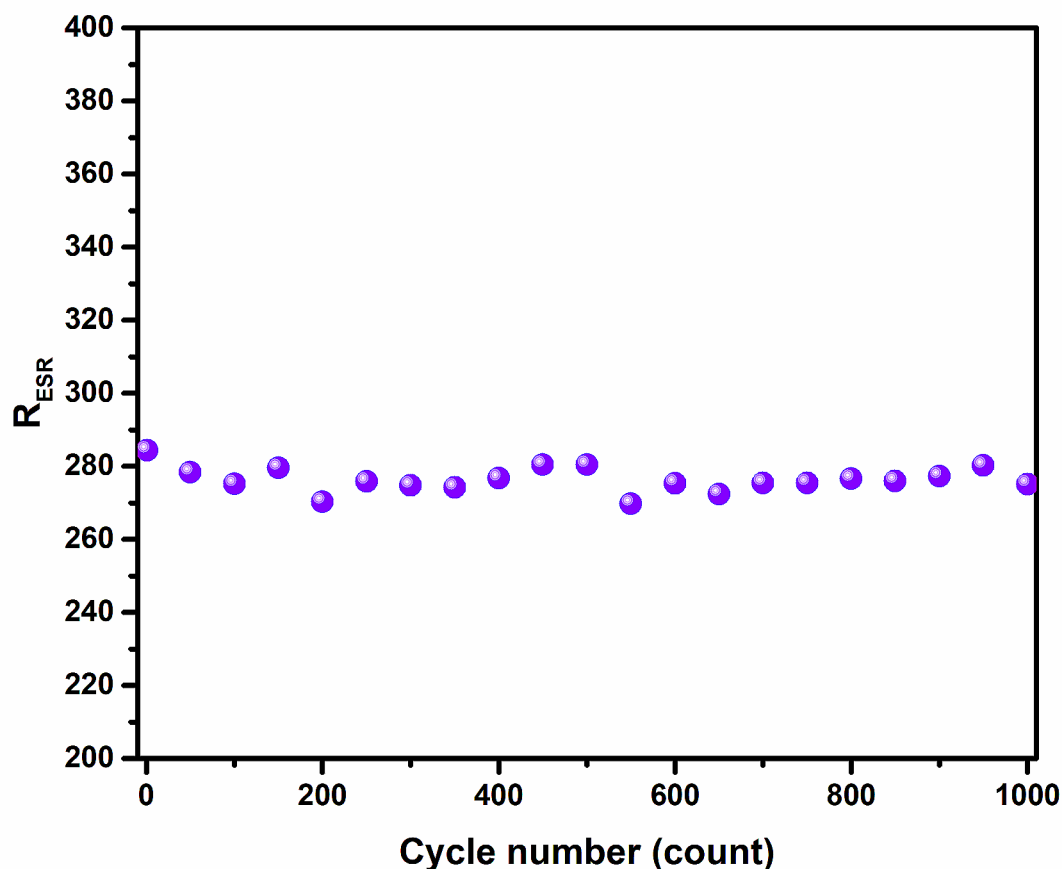


Fig. 17 The ESR value against cycle numbers up to 1000 cycles

Acknowledgements We gratefully acknowledge the International Research Centre (IRC), Kalasalingam Academy of Research and Education, for providing facilities and equipment to carry out the research.

Author Contributions All authors contributed to the study conception and design. Material preparation, data collection, and analyses were performed by M.Nandhinilakshmi. The first draft of the manuscript was written by Dr. D.Vanitha and all authors commented on previous versions of the manuscript. All authors read and approved the final manuscript.

Funding Ms. M.Nandhinilakshmi has received the technical and financial support from Kalasalingam Academy of Research and Education.

Data Availability No datasets were generated or analysed during the current study.

Declarations

Conflict of Interest On behalf of all authors, the corresponding author states that there is no conflict of interest.

Ethical Approval Not applicable.

References

1. Doagou-Rad S, Islam A, Merca TD (2020) An application-oriented roadmap to select polymeric nanocomposites for advanced applications: a review. *Polym Compos* 41:1153–1189. <https://doi.org/10.1002/pc.25461>
2. Siwal SS, Zhang Q, Devi N, Thakur VK (2020) Carbon-based polymer nanocomposite for high-performance energy storage applications. *Polym (Basel)* 12:1–31. <https://doi.org/10.3390/polym12030505>
3. Aziz SB, Brza MA, Saed SR et al (2020) Ion association as a main shortcoming in polymer blend electrolytes based on CS:PS incorporated with various amounts of ammonium tetrafluoroborate. *J Mater Res Technol* 9:5410–5421. <https://doi.org/10.1016/j.jmrt.2020.03.067>
4. Li Q, Horn M, Wang Y et al (2019) A review of Supercapacitors based on graphene and redox-active Organic materials. *Mater (Basel)* 12:703. <https://doi.org/10.3390/ma12050703>
5. Saranya P, Vanitha D, Sundaramahalingam K, Nandhinilakshmi M (2023). *J Elastomers Plast.* <https://doi.org/10.1177/00952443231184608>

6. Nandhinilakshmi M, Vanitha D, Nallamuthu N et al (2024) Fabrication of symmetric Super Capacitor using Lithium-ion conducting IOTA Carrageenan-based Biopolymer Electrolytes. *J Polym Environ* 32:1150–1169. <https://doi.org/10.1007/s10924-023-03014-6>
7. Perumal P, Christopher Selvin P, Selvasekarapandian S et al (2019) Plasticizer incorporated, novel eco-friendly bio-polymer based solid bio-membrane for electrochemical clean energy applications. *Polym Degrad Stab* 159:43–53. <https://doi.org/10.1016/j.polyimdegradstab.2018.11.013>
8. Nandhinilakshmi M, Vanitha D, Nallamuthu N, Sundaramahalingam K, Saranya P (2023) Fabrication of symmetric super capacitor using lithium-ion conducting IOTA Carrageenan-based biopolymer electrolytes. *J Polym Environ*. <https://doi.org/10.1007/s10924-023-03014-6>
9. Selvalakshmi S, Vanitha D, Saranya P et al (2022) Structural and conductivity studies of ammonium chloride doped agar-agar biopolymer electrolytes for electrochemical devices. *J Mater Sci Mater Electron* 33:24884–24894. <https://doi.org/10.1007/s10854-022-09198-2>
10. Abdullah OG, Hanna RR, Salman YAK (2017) Structural, optical, and electrical characterization of chitosan: methylcellulose polymer blends based film. *J Mater Sci Mater Electron* 28:10283–10294. <https://doi.org/10.1007/s10854-017-6796-7>
11. Kiruthika S, Malathi M, Selvasekarapandian S et al (2019) Eco-friendly biopolymer electrolyte, pectin with magnesium nitrate salt, for application in electrochemical devices. *J Solid State Electrochem* 23:2181–2193. <https://doi.org/10.1007/s10008-019-04313-6>
12. Farhana NK, Omar FS, Shanti R et al (2019) Iota-Carrageenan-based polymer electrolyte: impact on ionic conductivity with incorporation of AmNTFSI ionic liquid for supercapacitor. *Ionics (Kiel)* 25:3321–3329. <https://doi.org/10.1007/s11581-019-02865-1>
13. Nandhinilakshmi M, Vanitha D, Nallamuthu N et al (2022) Investigation on conductivity and optical properties for blend electrolytes based on iota-carrageenan and acacia gum with ethylene glycol. *J Mater Sci Mater Electron* 33:21172–21188. <https://doi.org/10.1007/s10854-022-08925-z>
14. Saranya P, Vanitha D, Sundaramahalingam K et al (2023) Structural and electrical properties of cross-linked blends of Xanthan gum and polyvinylpyrrolidone-based solid polymer electrolyte. *Ionics (Kiel)* 29:5147–5159. <https://doi.org/10.1007/s11581-023-05219-0>
15. Yusof YM, Illias HA, Kadir MFZ (2014) Incorporation of NH₄Br in PVA-chitosan blend-based polymer electrolyte and its effect on the conductivity and other electrical properties. *Ionics (Kiel)* 20:1235–1245. <https://doi.org/10.1007/s11581-014-1096-1>
16. Abirami M, Saratha R, Shilpa R, Vinitha B (2020) Preparation and characterization of Guar gum-based solid biopolymer electrolyte doped with lithium bis(trifluoromethanesulphonyl)imide (LiTFSI) plasticized with glycerol. *Bull Mater Sci* 43:6–11. <https://doi.org/10.1007/s12034-020-02218-z>
17. Jenova I, Venkatesh K, Karthikeyan S, Madeswaran S, Aristatil G, Prabu Moni JSD (2021) Solid polymer electrolyte based on tragacanth gum-ammonium thiocyanate. *J Solid State Electrochem* 25:2371–2383. <https://doi.org/10.1007/s10008-021-05016-7>
18. Noor ISM, Majid SR, Arof AK et al (2012) Characteristics of gellan gum–LiCF₃SO₃ polymer electrolytes. *Solid State Ionics* 225:649–653. <https://doi.org/10.1016/j.ssi.2012.03.019>
19. Badwaik HR, Hoque A, Al, Kumari L et al (2020) Moringa gum and its modified form as a potential green polymer used in biomedical field. *Carbohydr Polym* 249:116893
20. Tavares FC, Dörr DS, Pawlicka A, Oropesa Avellaneda C (2018) Microbial origin xanthan gum-based solid polymer electrolytes. *J Appl Polym Sci* 135:1–6. <https://doi.org/10.1002/app.46229>
21. Siddig M, Adam H, Siddig A, Eltahir N (2013) Electrical and optical properties of two types of Gum Arabic. *Sudan Med Monit* 8:174. <https://doi.org/10.4103/1858-5000.133006>
22. Sharma G, Kumar A, Naushad M et al (2022) Gum Acacia-Cross-linked-Poly(acrylamide) hydrogel supported C₃N₄/BiOI heterostructure for remediation of noxious Crystal Violet Dye. *Mater (Basel)* 15:2549. <https://doi.org/10.3390/ma15072549>
23. Chai MN, Isa MIN (2013) Electrical characterization and Ionic Transport Properties of Carboxyl Methylcellulose-Oleic Acid Solid Polymer Electrolytes. *Int J Polym Anal Charact* 18:280–286. <https://doi.org/10.1080/1023666X.2013.767033>
24. Shukur MF, Ithnin R, Illias HA, Kadir MFZ (2013) Proton conducting polymer electrolyte based on plasticized chitosan – PEO blend and application in electrochemical devices. *Opt Mater (Amst)* 35:1834–1841. <https://doi.org/10.1016/j.optmat.2013.03.004>
25. Sampath Kumar L, Christopher Selvin P, Selvasekarapandian S (2021) Impact of lithium triflate (LiCF₃SO₃) salt on tamarind seed polysaccharide-based natural solid polymer electrolyte for application in electrochemical device. *Polym Bull* 78:1797–1819. <https://doi.org/10.1007/s00289-020-03185-5>
26. Jinisha B, Anilkumar KM, Manoj M et al (2017) Development of a novel type of solid polymer electrolyte for solid state lithium battery applications based on lithium enriched poly (ethylene oxide) (PEO)/poly (vinyl pyrrolidone) (PVP) blend polymer. *Electrochim Acta* 235:210–222. <https://doi.org/10.1016/j.electacta.2017.03.118>
27. Sampathkumar L, Christopher Selvin P, Selvasekarapandian S et al (2019) Synthesis and characterization of biopolymer electrolyte based on tamarind seed polysaccharide, lithium perchlorate and ethylene carbonate for electrochemical applications. *Ionics (Kiel)* 25:1067–1082. <https://doi.org/10.1007/s11581-019-02857-1>
28. Prabakaran P, Manimuthu RP, Gurusamy S, Sebasthian E (2017) Plasticized polymer electrolyte membranes based on PEO/PVdF-HFP for use as an effective electrolyte in lithium-ion batteries. *Chin J Polym Sci (English Ed)* 35:407–421. <https://doi.org/10.1007/s10118-017-1906-9>
29. Sudiarti T, Wahyuningrum D, Bundjali B, Made Arcana I (2017) Mechanical strength and ionic conductivity of polymer electrolyte membranes prepared from cellulose acetate-lithium perchlorate. In: *IOP Conference Series: Materials Science and Engineering*, pp 1–8
30. Yusof YM, Kadir MFZ (2016) Electrochemical characterizations and the effect of glycerol in biopolymer electrolytes based on methylcellulose-potato starch blend. *Mol Cryst Liq Cryst* 627:220–233. <https://doi.org/10.1080/15421406.2015.1137115>
31. Das R, Pattanayak AJ, Swain SK (2018) Polymer nanocomposites for sensor devices. *Polymer-based nanocomposites for energy and environmental applications*. Elsevier, NY, pp 205–218
32. Nandhinilakshmi M, Vanitha D, Nallamuthu N et al (2023) Fabrication of high-performance symmetrical supercapacitor using lithium iodide-based biopolymer electrolyte. *Ionics (Kiel)* 30:1031–1049. <https://doi.org/10.1007/s11581-023-05270-x>
33. Aziz SB, Hamsan MH, Kadir MFZ et al (2019) Development of polymer blend electrolyte membranes based on Chitosan: dextran with high ion transport properties for EDLC application. *Int J Mol Sci* 20:3369. <https://doi.org/10.3390/ijms20133369>
34. Chitra R, Sathya P, Selvasekarapandian S, Meyvel S (2020) Synthesis and characterization of iota-carrageenan biopolymer electrolyte with lithium perchlorate and succinonitrile (plasticizer). *Polym Bull* 77:1555–1579. <https://doi.org/10.1007/s00289-019-02822-y>
35. Cholant CM, Rodrigues MP, Peres LL et al (2020) Study of the conductivity of solid polymeric electrolyte based on PVA/GA blend with addition of acetic acid. *J Solid State Electrochem* 24:1867–1875. <https://doi.org/10.1007/s10008-020-04605-2>

36. Christopher Selvin P, Perumal P, Selvasekarapandian S et al (2018) Study of proton-conducting polymer electrolyte based on K-carrageenan and NH₄SCN for electrochemical devices. *Ionics (Kiel)* 24:3535–3542. <https://doi.org/10.1007/s11581-018-2521-7>
37. Rudhzhiah S, Rani MSA, Ahmad A et al (2015) Potential of blend of kappa-carrageenan and cellulose derivatives for green polymer electrolyte application. *Ind Crops Prod* 72:133–141. <https://doi.org/10.1016/j.indcrop.2014.12.051>
38. Moniha V, Alagar M, Selvasekarapandian S et al (2018) Conductive bio-polymer electrolyte iota-carrageenan with ammonium nitrate for application in electrochemical devices. *J Non Cryst Solids* 481:424–434. <https://doi.org/10.1016/j.jnoncrysol.2017.11.027>
39. Kesavan K, Mathew CM, Rajendran S, Ulaganathan M (2014) Preparation and characterization of novel solid polymer blend electrolytes based on poly (vinyl pyrrolidone) with various concentrations of lithium perchlorate. *Mater Sci Eng B* 184:26–33. <https://doi.org/10.1016/j.mseb.2014.01.009>
40. Teoh KH, Ramesh S, Arof AK (2012) Investigation on the effect of nanosilica towards corn starch-lithium perchlorate-based polymer electrolytes. *J Solid State Electrochem* 16:3165–3170. <https://doi.org/10.1007/s10008-012-1741-4>
41. Vanitha D, Bahadur SA, Nallamuthu N et al (2017) Electrical impedance studies on sodium ion conducting composite blend polymer electrolyte. *J Inorg Organomet Polym Mater* 27:257–265. <https://doi.org/10.1007/s10904-016-0468-6>
42. Sundaramahalingam K, Jayanthi S, Vanitha D, Nallamuthu N (2021) Dielectric studies of designed novel sodium-based polymer electrolyte with the effect of adding amino acid. *Ionics (Kiel)* 27:3919–3932. <https://doi.org/10.1007/s11581-021-04116-8>
43. Nandhinilakshmi M, Vanitha D, Nallamuthu N et al (2023) Structural, electrical behavior of sodium ion-conducting corn starch–PVP-based solid polymer electrolytes. *Polym Bull* 80:3793–3817. <https://doi.org/10.1007/s00289-022-04230-1>
44. Sundaramahalingam K, Nallamuthu N, Manikandan A et al (2018) Studies on sodium nitrate based polyethylene oxide / polyvinyl pyrrolidone polymer blend electrolytes. *Phys B Condens Matter* 547:55–63. <https://doi.org/10.1016/j.physb.2018.08.002>
45. Aziz SB, Al-Zangana S, Woo HJ et al (2018) The compatibility of chitosan with divalent salts over monovalent salts for the preparation of solid polymer electrolytes. *Results Phys* 11:826–836. <https://doi.org/10.1016/j.rinp.2018.10.040>
46. Shukur MF, Ibrahim FM, Majid NA et al (2013) Electrical analysis of amorphous corn starch-based polymer electrolyte membranes doped with LiI. *Phys Scr* 88:025601. <https://doi.org/10.1088/0031-8949/88/02/025601>
47. Jothi MA, Vanitha D, Bahadur SA, Nallamuthu N (2021) Proton conducting polymer electrolyte based on cornstarch, PVP, and NH₄Br for energy storage applications. *Ionics (Kiel)* 27:225–237. <https://doi.org/10.1007/s11581-020-03792-2>
48. Shukur MF, Ithnin R, Kadir MFZ (2016) Ionic conductivity and dielectric properties of potato starch-magnesium acetate biopolymer electrolytes: the effect of glycerol and 1-butyl-3-methylimidazolium chloride. *Ionics (Kiel)* 22:1113–1123. <https://doi.org/10.1007/s11581-015-1627-4>
49. Ramya CS, Selvasekarapandian S, Hirankumar G et al (2008) Investigation on dielectric relaxations of PVP-NH₄SCN polymer electrolyte. *J Non Cryst Solids* 354:1494–1502. <https://doi.org/10.1016/j.jnoncrysol.2007.08.038>
50. Abdullah OG, Hanna RR, Ahmed HT et al (2021) Conductivity and dielectric properties of lithium-ion biopolymer blend electrolyte based film. *Results Phys* 24:104135. <https://doi.org/10.1016/j.rinp.2021.104135>
51. Bhargav PB, Sarada BA, Sharma AK, Rao VVRN (2010) Electrical conduction and dielectric relaxation phenomena of PVA based Polymer electrolyte films. *J Macromol Sci Part Pure Appl Chem* 47:131–137. <https://doi.org/10.1080/10601320903458564>
52. Anandha Jothi M, Vanitha D, Nallamuthu N et al (2020) Investigations of lithium ion conducting polymer blend electrolytes using biodegradable cornstarch and PVP. *Phys B Condens Matter* 580:411940. <https://doi.org/10.1016/j.physb.2019.411940>
53. Woo HJ, Majid SR, Arof AK (2012) Dielectric properties and morphology of polymer electrolyte based on poly(ϵ -caprolactone) and ammonium thiocyanate. *Mater Chem Phys* 134:755–761. <https://doi.org/10.1016/j.matchemphys.2012.03.064>
54. Sudhakar YN, Selvakumar M (2013) Ionic conductivity studies and dielectric studies of poly(styrene sulphonic acid)/starch blend polymer electrolyte containing LiClO₄. *J Appl Electrochem* 43:21–29. <https://doi.org/10.1007/s10800-012-0493-2>
55. Ramesh S (2002) Dielectric behaviour of PVC-based polymer electrolytes. *Solid State Ionics* 152–153:291–294. [https://doi.org/10.1016/S0167-2738\(02\)00311-9](https://doi.org/10.1016/S0167-2738(02)00311-9)
56. Aziz SB, Karim WO, Brza MA et al (2019) Ion transport study in CS: POZ based Polymer membrane electrolytes using Trukhan model. *Int J Mol Sci* 20:1–20. <https://doi.org/10.3390/ijms20215265>
57. Ramly K, Isa MIN, Khair ASA (2011) Conductivity and dielectric behaviour studies of starch/PEO + x wt-%NH₄Cl polymer electrolyte. *Mater Res Innov* 15:s82–s85. <https://doi.org/10.1179/143307511X1303189074>
58. Manjuladevi R, Thamilselvan M, Selvasekarapandian S et al (2017) Mg-ion conducting blend polymer electrolyte based on poly(vinyl alcohol)-poly (acrylonitrile) with magnesium perchlorate. *Solid State Ionics* 308:90–100. <https://doi.org/10.1016/j.ssi.2017.06.002>
59. Selvasekarapandian S, Baskaran R, Hema M (2005) Complex AC impedance, transference number and vibrational spectroscopy studies of proton conducting PVAc-NH₄SCN polymer electrolytes. *Phys B Condens Matter* 357:412–419. <https://doi.org/10.1016/j.physb.2004.12.007>
60. Geiculescu OE, Rajagopal R, Creager SE et al (2006) Transport properties of solid polymer electrolytes prepared from oligomeric fluorosulfonimide lithium salts dissolved in high molecular weight poly(ethylene oxide). *J Phys Chem B* 110:23130–23135. <https://doi.org/10.1021/jp062648p>
61. Surulinathan A, Sambandam B, Pandikumar A (2020) Structural analysis and redox additive electrolyte based supercapacitor performance of ZnO/CeO₂ nanocomposite. *Mater Sci Semicond Process* 106:104. <https://doi.org/10.1016/j.mssp.2019.104765>
62. Aziz SB, Hamsan MH, Abdullah RM et al (2020) Protonic EDLC cell based on chitosan (CS): methylcellulose (MC) solid polymer blend electrolytes. *Ionics (Kiel)* 26:1829–1840. <https://doi.org/10.1007/s11581-020-03498-5>
63. Aziz S, Dannoun E, Abdulwahid R et al (2022) The study of Ion Transport Parameters in MC-Based Electrolyte membranes using EIS and their applications for EDLC devices. *Membr (Basel)* 12:139. <https://doi.org/10.3390/membranes12020139>
64. Aziz SB, Nofal MM, Kadir MFZ et al (2021) Bio-based Plasticized PVA Based Polymer Blend electrolytes and Electrochemical properties. *Mater (Basel)* 14:1994
65. Aziz SB, Hamsan MH, Brza MA et al (2019) Fabrication of energy storage EDLC device based on CS:PEO polymer blend electrolytes with high Li⁺ ion transference number. *Results Phys* 15:102584. <https://doi.org/10.1016/j.rinp.2019.102584>
66. Hadi JM, Aziz SB, Saeed SR et al (2020) Investigation of ion transport parameters and electrochemical performance of plasticized biocompatible chitosan-based proton conducting polymer composite electrolytes. *Membr (Basel)* 10:1–27. <https://doi.org/10.3390/membranes10110363>

Publisher's Note Springer Nature remains neutral with regard to jurisdictional claims in published maps and institutional affiliations.

Springer Nature or its licensor (e.g. a society or other partner) holds exclusive rights to this article under a publishing agreement with the author(s) or other rightsholder(s); author self-archiving of the accepted manuscript version of this article is solely governed by the terms of such publishing agreement and applicable law.